ELSEVIER

Contents lists available at ScienceDirect

Applied Energy

journal homepage: www.elsevier.com/locate/apenergy





A closed-loop integration of scheduling and control for hydraulic fracturing using offset-free model predictive control

Kaiyu Cao, Sang Hwan Son, Jiyoung Moon, Joseph Sang-Il Kwon

Texas A&M Energy Institute, Texas A&M University, College Station, Texas 77845, United States
Artie McFerrin Department of Chemical Engineering, Texas A&M University, College Station, Texas 77845, United States

ARTICLE INFO

Keywords: Shale gas Hydraulic fracturing Integrated scheduling and control Offset-free model predictive control Pumping profile

ABSTRACT

As the development of shale gas resources has to be accelerated to satisfy the increasing global natural gas demand, many optimization approaches have been developed to handle the complexity associated with the shale gas system and discern the optimal design and operation strategy. However, it is worth mentioning that the essential hydraulic fracturing operation has not been considered as a dynamic process in the previous studies, which may lead to suboptimal solutions. Motivated by this consideration, we first develop an integrated model to simultaneously consider the scheduling and control of hydraulic fracturing operations to enhance the economic performance of the shale gas system. In particular, a reduced-order model is developed and integrated with the scheduling model to reduce the model complexity. To cope with the plant-model mismatch of the reduced-order model, we propose an online integrated framework with two feedback loops. In the outer loop, the integrated model is solved to determine the scheduling decisions and controller references. Then, an offset-free model predictive control system is designed to track the references online in the inner loop. By utilizing the offset-free model predictive control scheme, the tracking performance is enhanced and the plant-model mismatch is compensated for, which helps avoid dramatic changes in the solutions obtained by re-solving the integrated problem online. The effectiveness of the proposed online integrated framework is demonstrated by considering a hypothetical case study based on Marcellus Shale Play. It shows that the undesirable performance degradation induced by the plant-model mismatch can be decreased by the developed offset-free model predictive control system, and the overall economic performance of the shale gas system is improved with the proposed approach.

1. Introduction

The global increase in energy demand, paired with the resultant growth of environmental pollution, has accelerated the development and utilization of natural gas. In this regard, shale gas, which is natural gas trapped within the porous sedimentary rock, is now promising and expected to be an indispensable resource to meet the increasing global energy demand [1]. Specifically, an essential step of shale gas extraction is the hydraulic fracturing process, which creates high conductivity pathways and enhances the permeability of stimulated volume to unlock the gas trapped in the rock [2]. However, one big concern associated with this operation is that it demands a huge amount of water to formulate the fracturing fluid, which may overburn the local water sources. To fracture a typical shale gas well, around 190 to 38,000 m³ of fracturing fluid is used, depending on shale gas formation [3]. Besides,

after the well is completed, a certain amount of the injected fracturing fluid is recovered in the first few weeks as wastewater; the wastewater continues to be generated over the entire production stage due to the formation brine coproduced with shale gas. Such wastewater is characterized by high salinity and high concentration of various contaminants, which may pollute the streams when being discharged [3]. On top of this, the opened wells release methane into the air, which is about 25 times more potent as a greenhouse gas (GHG) than carbon dioxide. Some of the midstream (e.g., shale gas processing) and downstream operations (e.g., power generation) involved in the shale gas production system could also incur a large amount of GHG emissions [4]. Thus, one common challenge in the shale gas industry is to manage the operations of shale gas production system in a unified and optimal manner while simultaneously taking into account both the economic and environmental criteria. Given the significant role that shale gas plays in the energy industry, a considerable number of optimization studies have

^{*} Corresponding author at: Texas A&M Energy Institute, Texas A&M University, College Station, Texas 77845, United States. E-mail address: kwonx075@tamu.edu (J.S.-I. Kwon).

Nomenclature		ys_i	indicates if freshwater impoundment at wellpad \boldsymbol{i} is constructed
Sets I	{i I is a wellpad}	$ysu_{i,t}$	indicates if freshwater impoundment constructed at
			wellpad i is used in time period t
F	{f f is a freshwater source}	Continuo	us Variables
R	{r r is a underground reservoir}		
T	{t t is a time period/point}	$\mathit{fw}_i^{\mathit{wellpad}}$	freshwater demand at wellpad <i>i</i> in each week,m ³
ST	{st st is a pumping stage}	$fwd_{i,t}$	freshwater demand at wellpad i in time period t ,m ³
K	{k k is a time step}	$pump_{f,i,t}$	flowrate of freshwater from freshwater source f to wellpad i in time period t ,m ³ •week ⁻¹
Paramete	rs	storefw _{i.t}	level of water in freshwater impoundment at wellpad i in
ϕ	proppant bank porosity	$storej w_{i,t}$	
$ ho_{sd}$	proppant particle density,kg/m ³		time period t ,m ³
α	maximum close-packed proppant volume fraction	$v f w_i$	capacity of freshwater impoundment at wellpad <i>i</i> ,m ³
h_{eq}	equilibrium proppant bank height,m	$sg_{i,t}^{wellpad}$	shale gas production forecast at wellpad <i>i</i> in time period
FracD _i	operation time for hydraulic fracturing at wellpad <i>i</i> ,week		t , m^3 •week $^{-1}$
TD	transition time for moving the fracturing crew between	ean	shale gas production at wellpad i in time period
12	two wellpads, week	$sgp_{i,t}$	
OD_i	time required to obtain steady flow of shale gas production		t ,m 3 •week $^{-1}$
OD_i		$\mathit{sgsell}_{i,t}$	shale gas production at wellpad <i>i</i> that is directly sold to the
	after the completion of hydraulic fracturing operation at		market in time period $t, m^3 \cdot week^{-1}$
a opmax	wellpad i, week	$sginj_{i,r,t}$	shale gas production at wellpad <i>i</i> that is temporarily
SCP^{max}	allowed maximum capacity of freshwater	8 71,7,2	injected into underground reservoir r in time period
	impoundment,m ³		$t,$ m $^3 \cdot$ week $^{-1}$
avai $l_{f,t}$	water availability in freshwater source f in time period	injection	t_{t} shale gas production that is temporarily injected into
	t,m^3 •week $^{-1}$	injection _r	
RCP_r^{max}	allowed maximum capacity of underground reservoir r , m^3		underground reservoir r in time period t ,m ³ •week ⁻¹
Demand _t ^m		$storesg_{r,t}$	level of shale gas in underground reservoir r in time period
Demana _t	$t, m^3 \cdot \text{week}^{-1}$		<i>t</i> ,m ³
		withdraw	$al_{r,t}$ shale gas production that is withdrawn from
$Demand_t^m$			underground reservoir r in time period t ,m ³ •week ⁻¹
	t ,m 3 •week $^{-1}$	output 1_t	shale gas production that is directly sold to the market in
FWQ^{max}	maximum flowrate of injected hydraulic fracturing fluid in	outputIt	time period t ,m ³ •week ⁻¹
	each pumping stage,m ³ ·s ⁻¹	or strong to	
FWQ^{min}	minimum flowrate of injected hydraulic fracturing fluid in	$output2_t$	shale gas production that is withdrawn from underground
1 W Q	each pumping stage,m³•s ⁻¹		reservoir r and then sold to the market in time period
Draga Cmax			t ,m 3 •week $^{-1}$
$PropC^{max}$	maximum proppant concentration of injected hydraulic	$output_t$	total shale gas production that is sold to the market in time
	fracturing fluid in each pumping stage		period t ,m ³ •week ⁻¹
$PropC^{min}$	minimum proppant concentration of injected hydraulic	$x_{i,st,k}$	hydraulic fracturing dynamic system state in pumping
	fracturing fluid in each pumping stage	3	stage st and at time step k at wellpad i
F_0	freshwater demand for pad time,m ³	$u_{i,st}$	hydraulic fracturing dynamic system input in pumping
T_{stage}	time for each pumping stage,s	1,51	stage st at wellpadi
N_i	number of fractures per stage at wellpadi	V	hydraulic fracturing dynamic system output in pumping
R_i	completion rate at wellpad i , $stages \cdot week^{-1}$	$y_{i,st,k}$	stage st at wellpadi
C_i^{drill}		-	-
	drilling cost for wellpad i,\$	$q_{i,st}$	flowrate of injected hydraulic fracturing fluid in pumping
C_i^{prod}	unit shale gas production cost at wellpad i ,\$•m ⁻³		stage <i>st</i> at wellpad $i,m^3 \cdot s^{-1}$
C_f^{pump}	water withdrawal cost,\$•m ⁻³	$c_{i,st}$	proppant concentration of injected hydraulic fracturing
C^{propac}	proppant acquisition cost,\$•kg ⁻¹		fluid in pumping stage st at wellpadi
Csto_base	base investment cost required to construct a freshwater	$W_{i,st,k}^{avg}$	average fracture width in pumping stage st and at time step
C	impoundment,\$.,,.	k at wellpad i, m
Csto_incre	•	$W_{i,st,k}^{wellbore}$	fracture width at the wellbore in pumping stage <i>st</i> and at
Cam-mere	unit incremental investment cost for a freshwater	i,st,k	
	impoundment, $\$ \cdot m^{-3}$	7	time step k at wellpad i, m
C^{sto_oper}	unit operating cost for a freshwater	$L_{i,st,k}$	fracture length in pumping stage st and at time step k at
	impoundment,\$•week ⁻¹	_	wellpad i, m
$C_r^{injection}$	unit injection cost at underground reservoir r , \$•m ⁻³	$W_i^{propped}$	average propped fracture width at the end of closure at
$C_r^{withdrawal}$	unit withdrawal cost at underground reservoir r ,\$•m ⁻³		wellpad i, m
		$L_i^{propped}$	propped fracture half-length at the end of closure at
R_t^{gas1}	forecast of shale gas selling price in time period <i>t</i> inside the	<i>-</i> 1	wellpad i,m
	one-year scheduling horizon,\$•m ⁻³	c fracture	
R^{gas2}	forecast of shale gas selling price outside the one-year	$\mathit{fw}_i^{\mathit{fracture}}$	freshwater demand to simulate a single fracture at wellpad
	scheduling horizon,\$•m ⁻³		i,m ³
		$prop_i^{fractur}$	e proppant demand to simulate a single fracture at wellpad
Binary va	riables	r · · · r i	i,kg
$w_{i,t}$	indicates if hydraulic fracturing operation at wellpad w	, wellpa	
	starts in time periodt	$prop_i^{wellpas}$	total proppant demand to complete wellpad i,kg

 $\begin{array}{c} \textit{cumsg}_i^{\textit{fracture}} \quad \text{cumulative shale gas production of the first year from a} \\ & \text{single fracture at wellpad } i, \text{m}^3 \\ \textit{sg}_{i,t}^{\textit{fracture}} \quad \text{shale gas production forecast from a single fracture at} \\ & \text{wellpad } i \text{ in time period } t, \text{m}^3 \cdot \text{week}^{-1} \\ \textit{adtotalsg}_i^{\textit{wellpad}} \quad \text{total shale gas production out of the scheduling} \\ & \text{horizon at wellpad } i, \text{m}^3 \\ \textit{y}_i^{\textit{well}} \quad \text{indicates whether wellpad } i \text{ is fractured} \\ \textit{Profit} \quad \text{gross profit of the shale gas system,} \$ \\ \textit{Revenue}^{\textit{gas}} \quad \text{revenue from selling the shale gas production,} \$ \end{array}$

 $Revenue_1^{gas}$ revenue from selling the shale gas production inside the one-year scheduling horizon,\$ Revenue^{go} revenue from selling the shale gas production outside the one-year scheduling horizon,\$ $Cost^{drill}$ drilling, completion, and production costs,\$ $Cost^{fw}$ freshwater cost,\$ Cost^{prop} proppant cost,\$ Cost^{storefw} freshwater impoundment cost,\$ Cost^{storesg} underground reservoir cost,\$

been carried out both in academia and industries to discern the optimal design and operations of complex shale gas systems by considering the various time-scales: (1) the optimal network structure and drilling strategy are determined, while simultaneously considering shale gas supply chain network design [5-7], integration of water management and shale gas supply chain [8-11], life cycle analysis of shale gas development [4,12]; (2) the optimal schedule for specific operation(s) are computed, which includes the drilling and fracturing [13], turning in line [14], shut-in [15,16], refracturing [17,18], and four sequential operations [19]; and (3) the optimal well placement [20-22] or operation techniques [23,24] are obtained for maximized well performance. From the optimization point of view, it is necessary to integrate these divided decision layers while considering the process dynamics that directly influence the fracture conductivity and shale gas production rate. However, while the shale gas supply chain network is generally constructed over more than a decade, the process control (i.e. flowrate and proppant concentration of the injected hydraulic fracturing fluid) which affects the proppant distribution inside the created fractures, is generally considered in the period of seconds [2,25–27]. In this regard, it is imperative to develop a framework where the scheduling and control of hydraulic fracturing can be integrated appropriately, and the information can be exchanged between them accurately and efficiently for better economic benefits.

For integrated scheduling and control, initial efforts have been made following an intuitive method of including the dynamic model of the process as an additional set of constraints in the scheduling model; specifically, the simultaneous approach [28,29] and sequential approach [30,31] are commonly used to solve the resulting integrated model. However, this open-loop optimization disregards the possible disturbances in both the scheduling (e.g., unit breakdown) and control layers (e.g., fluctuation in input) which could immediately disrupt the production system. Thus, online integration of scheduling and control has been suggested to ensure the stability and performance of the process out of the nominal operating condition by rejecting disturbances during process operation, which consequently ensures the successful

implementation of designed schedules. However, such online integration demands that the frequency of solving the integrated problem should be comparable to the frequency of receiving feedback measurements in the control system in order to provide closed-loop stability and disturbance rejection [32]. In this regard, many approaches have been proposed to reduce the computational requirement (e.g., Lagrangean Decomposition [33], Bender's Decomposition [34,35], bilevel decomposition [36], back-off decomposition [37], multiparameteric MPC [38,39], and fast MPC [40]). On the other hand, since the fracturing process is regarded as a batch process that never reaches a steady-state, a dynamic model has to be built for each task executed in a processing unit, unlike in a continuous operation [35]. Owing to such fundamental differences in the integrated problem formulations, the number of dynamic models in the integration problem for a batch process is generally much higher than the one for a continuous process. Hence, the integration of scheduling and control for the batch systems has been less discussed due to the model complexity [41]. Moreover, studies to handle process disturbances while solving the integrated problem have been very rarely discussed.

In order to address the aforementioned problems, several approaches have been suggested. Zhuge and Ierapetritou [42] proposed a closedloop strategy for integrated scheduling and control problem to account for the presence of disturbances in process. In their work, the integrated problem was resolved once a deviation of the measured state from the reference value is larger than a threshold, with which the effects of disturbances can be eliminated. The same authors improved their work by using a fast MPC scheme [40]. A piecewise affine approximation of the process dynamics was developed and integrated with the scheduling level for computational efficiency. Further, a fast MPC scheme was used to track the reference states generated from the integrated model. In the online implementation, small disturbances were efficiently handled by the fast MPC while the integrated problem was reoptimized to cope with large disturbances. Furthermore, Chu and You [43] proposed an online implementation strategy for sequential batch processes, and similarly, the state reference determined by solving

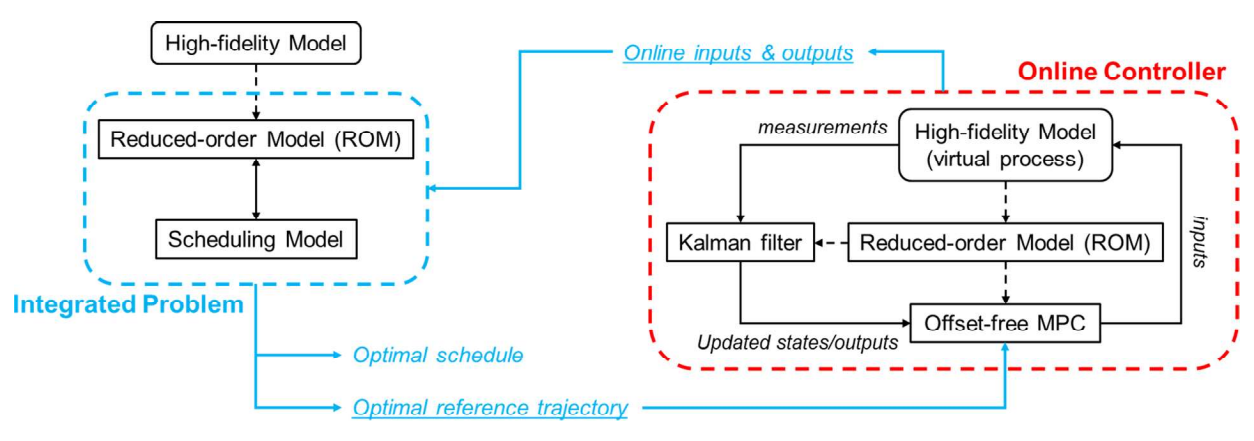


Fig. 1. Closed-loop integration of scheduling and control.

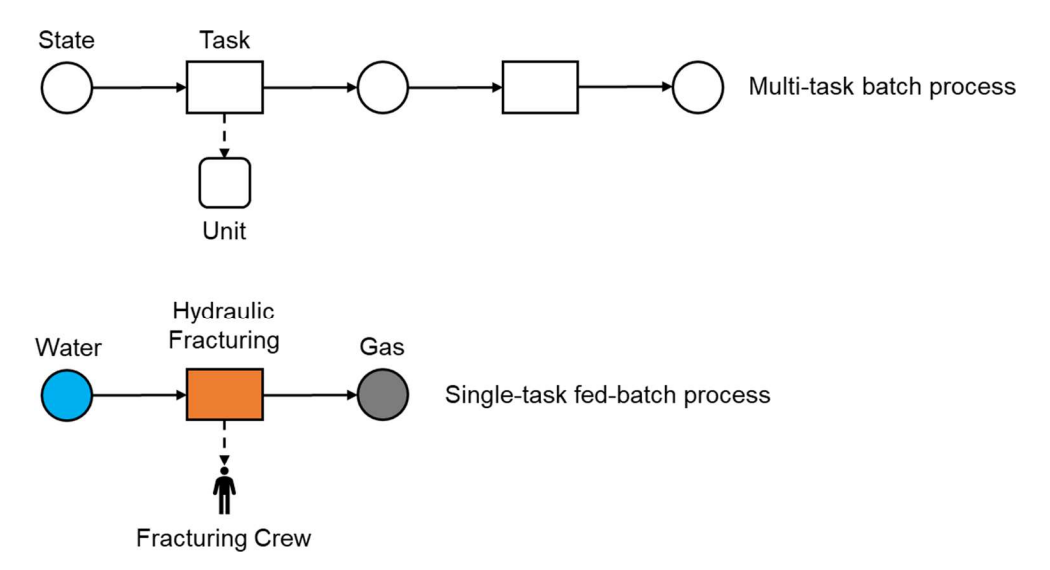


Fig. 2. Batch representation of hydraulic fracturing operation.

the integrated problem was tracked using a MPC system. Re-solving the integrated problem online is also considered necessary to handle the control system disruption and the processing unit breakdown. However, these studies have not considered how the controllers should be designed to track the determined references. Specifically, few of them considered that the negative impact caused by plant-model mismatch and unknown disturbances on the reference tracking performance of the controller could be alleviated or even completely eliminated through a careful controller design. Therein, the changes in the solutions by resolving the integrated problem are less dramatic; or, it is even possible that re-solving the integrated problem online becomes not necessary if only minor disturbances occur, which helps facilitate the online implementation and assure rescheduling stability [43]. To handle plant-model mismatch and unknown disturbances, offset-free MPC can be regarded as one of the most representative and systematic approaches in the control community. By augmenting the system state with disturbances and estimating the disturbance-augmented system state based on measurements, the effect from plant-model mismatch and unknown disturbances can be compensated for, and thus the zero-offset tracking objective can be achieved [44,45].

Motivated by these considerations, we propose a generalized framework for integrated scheduling and control (Fig. 1), which contains two levels of feedback loops, and apply it to hydraulic fracturing. At first, a reduced-order model (ROM) representing the original process dynamics is developed based on high-fidelity simulation data and integrated with the scheduling model to formulate the integrated problem. In the outer loop, the integrated problem is solved to simultaneously determine both the optimal schedule and the reference trajectories for every task, the latter of which is then transferred to the inner loop for the control problem. In the inner loop, for the task to be operated according to the optimal schedule, a Kalman filter is utilized for state estimation, and then an offset-free MPC system is designed to compute the exact control solution online for enhanced tracking performance while compensating for the plant-model mismatch and unknown disturbances. After the control system is solved, the values of the obtained manipulated input variables and output variables (i.e., which include all operational information necessary for the integrated problem) for the completed task are sent back to the outer loop as feedback information; then, the integrated problem is re-solved online, and the scheduling and control decisions for the remaining unoperated tasks are updated accordingly. Note that these two loops correspond to different models as well as different time scales. Specifically, the integrated model in the outer loop is event-based (i.e., it is re-solved when a task is completed) and solved in the order of weeks; on the other hand, the control systems in the inner loop are solved much more frequently than the integrated model (e.g., in the order of seconds). This actually facilitates the online implementation since there is no need to solve the integrated model at every controller sampling time. Besides the integration structure, there are some benefits of using the proposed framework: (1) the proposed approach is applicable to a dynamic market environment (e.g., varying product demand and price) since whenever the integrated problem is resolved online, the latest market information can be incorporated; (2) the developed ROM is not required to be significantly precise since the introduced offset-free MPC scheme has the ability to achieve zero-offset tracking. In this sense, this could lead to a computationally efficient integrated problem suitable for online implementation; and (3) with the offset-free MPC, the tracking performance can be significantly enhanced. In this sense, the dramatic change in the re-solving solution could be avoided and the frequency of re-solving the integrated model based on feedback information could be decreased.

The rest of the paper is organized as follows: The problem statement is defined in Section 2. In Section 3, the mathematical representation of the proposed integrated framework is described in detail. Section 4 explains the solution strategy. The results obtained from a hypothetical case study based on Marcellus Shale Play and the corresponding analysis are presented in Section 5. At the end, Section 6 summarizes the conclusions of the present work.

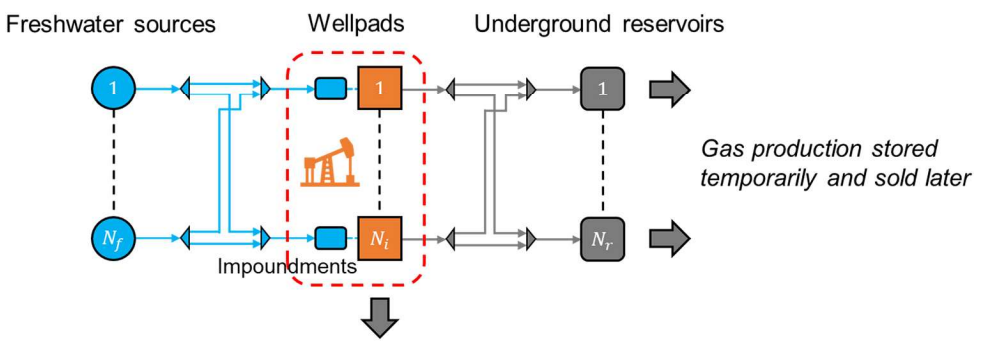
2. Problem statement

Hydraulic fracturing can be viewed as a fed-batch process: during the operation of a fracturing stage, freshwater and proppant are mixed and continuously injected into the wellbore. This treatment process is repeated until all the fracturing stages along the horizontal well are completed. After the whole process is completed, the production of shale gas can start. Thus, the scheduling part of the integrated problem can be formulated based on the State-Task Network (STN) representation for batch scheduling. Note that the states correspond to the amount of water fed into the wellpads or the amount of shale gas produced from the wellpads; the processing tasks correspond to the hydraulic fracturing operations at the wellpads [13]. As shown in Fig. 2, it can be presented as a single-task fed-batch process.

The problem addressed in this article can be stated as follows. The followings are given:

- The short-term scheduling horizon of interest;
- A set of identified candidate wellpads from which shale gas may or may not be extracted;

(a)



Gas production directly sold to the market

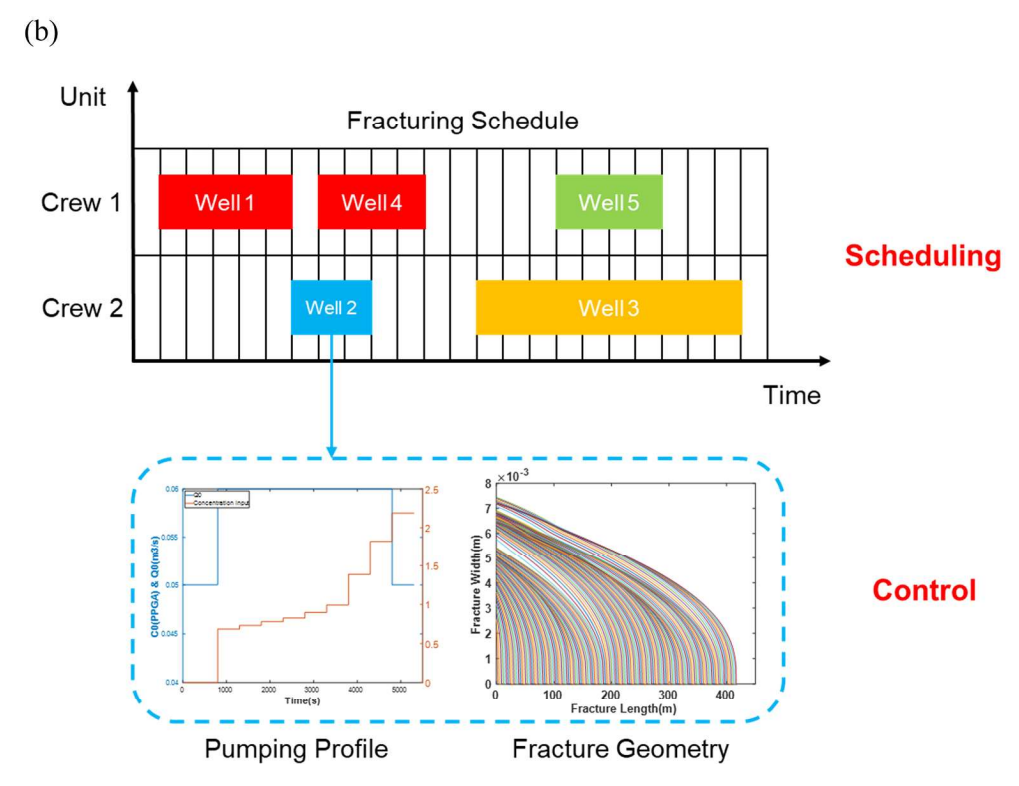


Fig. 3. Proposed integrated problem: (a) a superstructure of shale gas development; (b) decisions at the scheduling and control levels.

- The total number of fracturing stages and the number of fractures per stage for each wellpad;
- The number of drilling rigs and fracturing crews available for the gas extraction;
- The number of fracturing stages that can be completed per week (i.e., completion rate) by the fracturing crew for developing each wellpad;
- The transition time for transferring the fracturing crew from one wellpad to another wellpad;
- The operational constraints for the pumping profile (i.e., regarding the flowrate and proppant concentration of the injected hydraulic fracturing fluid; total number of pumping stages) implemented for hydraulic fracturing operations at each wellpad;
- A set of freshwater sources available to supply the water required to formulate fracturing fluid and the associated water availability in each time period;
- The cost of freshwater withdrawal in each time period;
- The maximum allowed capacity and number of freshwater impoundments, and the associated investment costs for construction

- costs (i.e., including base investment cost, incremental investment cost, and operating cost);
- The capacity and number of underground reservoirs available to temporarily store the extracted gas, and the corresponding operating costs (i.e., including injection cost and withdrawal cost);
- The sales price of natural gas in each time period;
- The cost of proppant (i.e., sand) acquisition in each time period;
- The drilling cost and unit shale gas production cost in each time period at each wellpad;
- The maximum and minimum natural gas demand in each time period.

The objective of the integrated problem is to schedule the hydraulic fracturing at wellpads to maximize the gross profit while satisfying the time-varying natural gas demand by accounting for the revenue of shale gas production and the costs of well drilling and completion, shale gas production, freshwater withdrawal and proppant acquisition, freshwater impoundment construction and use, and underground reservoir use. The goal is to determine the short-term fracturing schedule of the

Water Availability Dynamic modeling of hydraulic fracturing **Product Demand** Input/Output data Time-varying parameters Reduced-Order Model (ROM) CMG Map Scheduling Optimization Model Integrated Scheduling and Control Model Fracking Schedule: $w_{i,t}$ Re-solving Designed Pumping Profile: $q_{i,st}^{ref}$, $c_{i,s}^{re}$ (Online) Designed Fracture Geometry: $W_{i,st,k}^{avg,ref}$, $W_{i}^{propped,ref}$, $L_{i}^{propped,ref}$ Fracture Geometry under Control: $W_{i \text{ of } k}^{avg,online}$, $W_{i}^{propped,online}$, Shale Gas Production forecast: sg

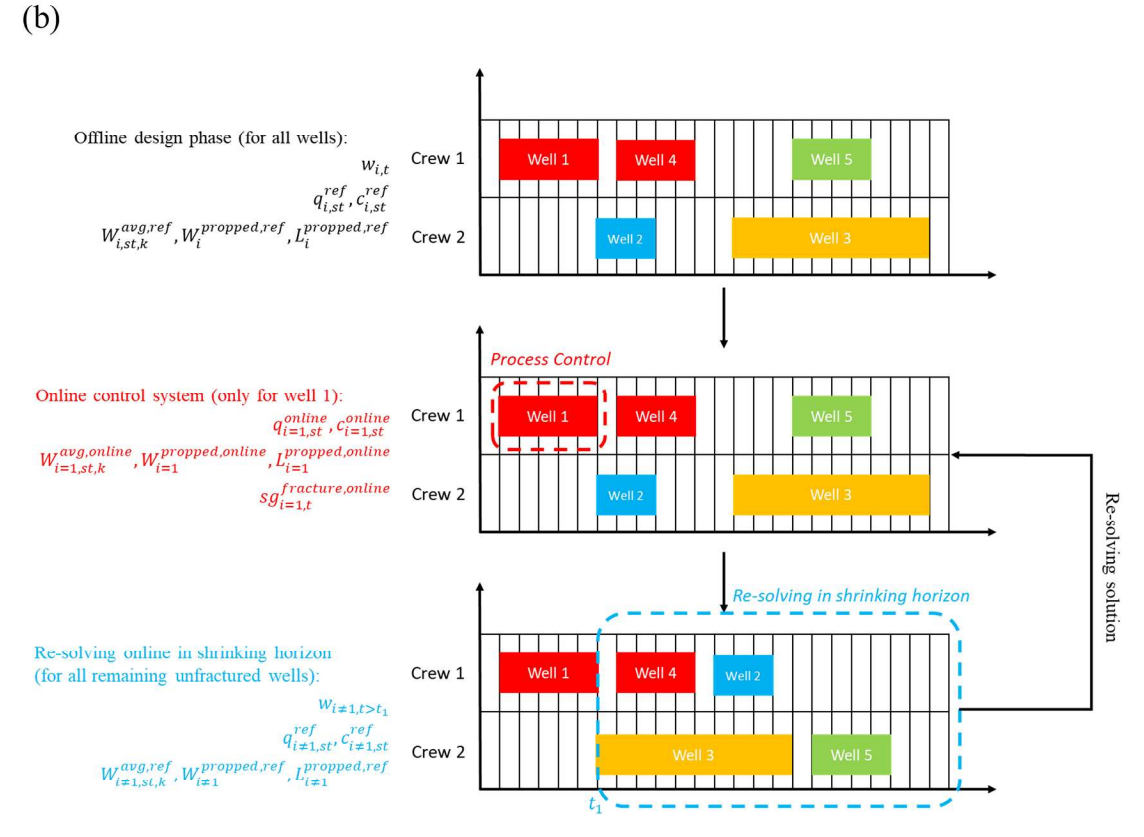


Fig. 4. Online integration of scheduling and control for hydraulic fracturing: (a) information flow between components; and (b) an illustrative example.

wellpads, the pumping profiles for the hydraulic fracturing operations at the wellpads, and the capacities of the freshwater impoundments to be constructed. For this purpose, a superstructure for the short-term shale gas development problem is proposed as shown in Fig. 3(a). Herein, the system comprises a set of wellpads $(I = \{i | i = 1, 2, \cdots N_i\})$, a set of freshwater sources $(F = \{f | f = 1, 2, \cdots N_f\})$, a set of underground reservoirs $(R = \{r | r = 1, 2, \cdots N_r\})$, and one drilling rig with one fracturing crew.

(a)

The information flow of the proposed closed-loop integration framework and an illustrative example is shown in Fig. 4. The outer loop

mainly uses the integrated scheduling and control model (i.e., the integrated problem) shown in Fig. 4(a). Specifically, the scheduling optimization model is at first formulated through a discrete-time MILP model, based on the STN representation for batch scheduling. Then, a ROM approximating the original hydraulic fracturing process dynamics is developed to represent the relationship between the pumping profile and the fracture geometry. Moreover, a map is developed using Computer Modeling Group (CMG) simulation data to forecast the corresponding shale gas production based on the fracture geometry. By incorporating the ROM and CMG map into the scheduling optimization

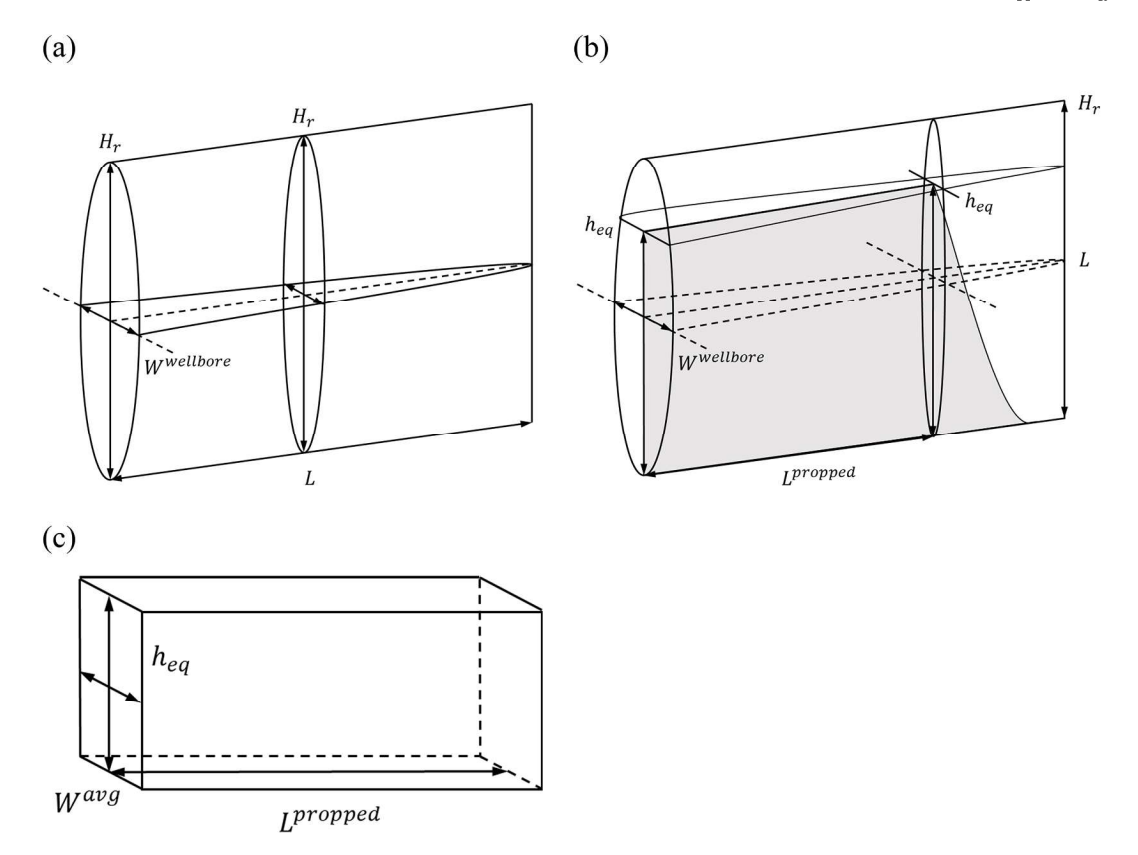


Fig. 5. (a) Fracture geometry at the end of pumping with the PKN model; (b) proppant bank at the end of pumping (the cross-sectional area is highlighted as the grey area); and (c) cube-approximation used in this work.

model as constraints, the integrated scheduling and control model can be formulated. Herein, the obtained integrated model becomes an MINLP model which simultaneously generates the optimal scheduling decisions (i.e., the fracking schedule, $w_{i,t}$) and the controller output reference trajectories (i.e., the designed average fracture width, $W_{i,st,k}^{avg,ref}$). Note that due to the inevitable disturbances in the real process, the integrated problem is used to determine the output references instead of process inputs; subsequently, the controller in the inner loop is utilized to compute the process inputs online that would track the output references obtained from the outer loop.

In hydraulic fracturing, it is important to make sure the output reference is tracked well (i.e., the designed average fracture width, $W_{i,st,k}^{avg,ref}$) to achieve the desired fracture geometry and thereby the desired shale gas production rate, with which the future shale gas demand can be satisfied and the gross profit of the shale gas system can be maximized. Since the average fracture width is unmeasurable in the real process, it should be estimated based on available real-time measurements through a Kalman filter. For computational efficiency, the developed ROM is used for the Kalman filter and MPC controller design in the inner loop. In the presence of the plant-model mismatch and unknown disturbances, the tracking performance of the online control system could be deteriorated which would cause the actual shale gas production to deviate largely from its target; it is another important reason why the control inputs should be separately computed by the inner loop. Specifically, the online control system is solved to generate the optimal control actions (i.e., the pumping profile, $q_{i,st}^{online}$ and $c_{i,st}^{online}$).

Once the hydraulic fracturing operation is completed, the process outputs (i.e., the actual fracture geometry, $W_{i,st,k}^{avg,online}$, $W_i^{propped,online}$, and $L_i^{propped,online}$) can be measured. With the actual fracture geometry, the corresponding shale gas production ($sg_{i,r}^{fracture,online}$) can be calculated, which should be sent back to the integrated problem in the outer loop as

the feedback information. Furthermore, since a large amount of water requirement is one of the biggest issues associated with hydraulic fracturing, the actual freshwater consumption ($fw_i^{wellpad,online}$) is also sent back as feedback. Once the feedback information is received, the integrated problem will be re-solved online to update the scheduling decisions and controller output references accordingly.

Considering an illustrative generalization of the shale gas development example, some assumptions are made particularly in this study for simplification, which are follows:

- The fixed scheduling horizon is discretized into weeks as time intervals:
- Each wellpad contains multiple shale gas wells; however, they are assumed aggregated so that they have to be all stimulated before the fracturing crew is transferred to another wellpad;
- All the wellpads share the same geological characteristics;
- Each wellpad is connected to exactly one nearby freshwater impoundment through piping;
- The freshwater impoundments are constructed at the beginning of the scheduling horizon with fixed capacity;
- The set of freshwater sources are seasonal, interruptible sources and their corresponding water availability is given based on historical flowrate data;
- Proppant is directly purchased from the market and thus no associated resource availability, storage, and transport problems are considered:
- Each pipeline segment has enough capacity to transport freshwater and gas production in each time period;
- The considered potential shale gas development area is small. Thus, only one drilling rig and one fracturing crew is available to handle all the wellpads; no transportation cost is considered in the objective function;

- The pumping profile designs for the hydraulic fracturing operations at the same wellpad are the same;
- · Wastewater production and reuse are not considered;
- Shale gas production from each wellpad starts after all the fracturing stages in the wellpad are completed. In addition, one week is required after the hydraulic fracturing operations of the entire wellpad are completed and before the opened wells begin to produce a steady flow of shale gas (i.e., it can be explained as a period of time for turning in line operation [19]).

3. Mathematical model formulation

In this section, the detailed description of the mathematical model is presented. As shown in Fig. 4, the online integrated framework can be divided into three sections. First, the integrated problem that is solved in the outer loop to obtain the fracturing schedule and output reference trajectories is presented. Specifically, the models used to represent the hydraulic fracturing process (i.e., development of ROM and CMG simulation) are elucidated in Section 3.1, and Section 3.2 describes the mathematical representation of the integrated scheduling and control model for hydraulic fracturing. Then, the offset-free MPC system that is solved online to track the output references is designed in Section 3.3. Finally, the re-solving part based on the feedback information (i.e., the actual pumping profile and shale gas production forecast for the last completed wellpad) from the inner loop is shown in Section 3.4.

3.1. Hydraulic fracturing process model

A hydraulic fracturing process is characterized by three subprocesses: fracture propagation, proppant transport, and proppant bank formation. To develop the high-fidelity hydraulic fracturing process model, the fracture propagation process is described using the Perkins, Kern, and Nordgren (PKN) model. During the pumping process, the fracture grows and thus its width at the wellbore (Wwellbore) and length (L) increase over time. According to the assumptions for PKN model, the resulting fracture at the end of pumping should have a rectangular fracture shape and elliptical fracture cross-sectional area, which is presented in Fig. 5(a). On the other hand, since a low-viscosity fracturing fluid is generally used for the operation of shale wells, most of the injected proppant do not stay in suspension in the created fracture during the pumping process; instead, they settle at the bottom of the fracture quickly and form a proppant bank. As the fracture propagates, the proppant bank also grows and thus its height increases over time. Particularly, when its height reaches the equilibrium height (i.e., a state when the rate of proppant washout on top of the proppant bank is equal to the rate of bank formation via proppant settling [2]), the newly injected proppant particles will directly flow over the portion of the proppant bank with equilibrium height and settle at a location where the proppant bank has not reached the equilibrium height yet. Thus, the length of the proppant bank also increases over time. Fig. 5(b) presents a cross-sectional area of the proppant bank formed at the end of pumping. Note that h_{eq} represents the equilibrium height of the proppant bank and $L^{propped}$ represents the length of the proppant bank with the height as h_{eq} . Please refer to Siddhamshetty et al. [2] for more details regarding the assumptions and dynamic modeling work. After solving the process model, we are able to obtain the evolution of fracture length and fracture width, and the spatiotemporal profiles of proppant concentration and proppant bank height during the hydraulic fracturing process.

However, due to the significant computational complexity of the developed high-fidelity process model, a reduced-order model (ROM) is necessary for the purpose of scheduling optimization, model predictive control design, and state estimator. Thus, the high-fidelity process model is viewed as a virtual hydraulic fracturing process to generate the input/output data. Based on the obtained open-loop simulation data, the multivariable output error state-space (MOESP) algorithm is used to

develop a linear time-invariant state-space model of the hydraulic fracturing process, as presented in Eqs. (1) and (2).

$$x(t_{k+1}) = Ax(t_k) + Bu(t_k)$$
(1)

$$y(t_k) = Cx(t_k) \tag{2}$$

where the A, B, and C are parameter matrices determined by the MOESP algorithm, $x(t_k)$ are the system states, and $u(t_k)$ and $y(t_k)$ are a set of the manipulated input variables and output variables at time point t_k , respectively. Specifically, the input variables are the flowrate $(q(t_k))$ and proppant concentration $(c(t_k))$ of injected fracturing fluid at the wellbore. Additionally, the output variables are the average fracture width over the optimal fracture half-length $(W^{avg}(t_k))$, the fracture width at the wellbore $(W^{wellbore}(t_k))$, and the fracture length $(L(t_k))$. Note that in practice, the reliable real-time measurements are only the fracture width at the wellbore and the fracture length. Thus, the unmeasurable average fracture width needs to be estimated through a Kalman filter, which will be discussed in Section 3.3 for the design of the control system.

After the pumping process is stopped, the fracturing fluid remained in the created fracture will leak off to the formation and the proppant will be trapped by the closing fracture walls, due to the natural stress in the formation (i.e., which is called the closure process). It is assumed that a uniform proppant distribution in the formulated proppant bank is achieved; also, it is assumed that all the proppant will reach the close-packed state after the closure process. Thus, at the end of the closure process, the local proppant concentration will all reach the maximum close-packed concentration which is taken as 0.65 in this study [46]. Based on the known average fracture width at the end of pumping (W^{avg}) the averaged propped fracture width at the end of closure ($W^{propped}$) can be calculated using Eq. (3).

$$(1 - \phi)W^{avg} = \alpha W^{propped} \tag{3}$$

where ϕ is the proppant bank porosity, and α is the maximum close-packed proppant volume fraction. Note that when calculating the average fracture width, the fracture shape is approximated as a cube to simplify the fracture structure (i.e., the cube-approximation as illustrated in Fig. 5(c)). Specifically, only the fracture whose proppant bank height is greater than or equal to the equilibrium height is considered as effective for shale gas production (i.e., the effective fracture). Thus, the propped fracture half-length of the resulting effective fracture ($L^{propped}$) can be easily computed by Eq. (4), based on the fixed proppant amount and obtained averaged propped fracture width.

$$L^{propped} = prop^{fracture} / (2\rho_{sd} h_{eq} \alpha W^{propped})$$
(4)

where ρ_{sd} is the proppant particle density, $prop^{fracture}$ is the proppant amount for one fracture, and h_{eq} is the equilibrium proppant bank height.

After obtaining the propped fracture length and calculating the average propped fracture width, we incorporated them into CMG, which is a reservoir simulation software, to predict the corresponding shale gas production over several years. The necessary parameters (e.g., reservoir dimension, bottomhole pressure, etc.) are mainly taken from Mao et al. [46]. After the model validation, a set of different propped fracture geometries is used as the inputs to the CMG-GEM module (i.e., an advanced compositional and unconventional simulator) to generate the corresponding daily shale gas production rates. With the simulation data, maps can be generated to represent the relationship between the propped fracture geometry and shale gas production rate, which are necessary to formulate the integrated scheduling and control model as illustrated in Fig. 4(a).

3.2. Integrated scheduling and control model for hydraulic fracturing

The scheduling optimization model for hydraulic fracturing is formulated as an MILP model, which involves the assignment

constraints, logic constraints, material balances, and an objective function. As explained in Section 2, by incorporating the developed ROM and CMG map into the scheduling optimization model as additional constraints, the integrated scheduling and control model can be formulated, which is an MINLP problem. The main decision variables are the binary variables that indicate the fracturing schedule of chosen wellpads and the continuous variables that indicate the corresponding pumping profiles and fracture geometries for hydraulic fracturing operations.

3.2.1. Constraints at scheduling level

Assignment constraint

Eq. (5) specifies that, within the scheduling horizon, each wellpad i can only be fractured once by the fracturing crew in a given time period t

$$\sum w_{i,t} \le 1 \qquad \forall i \tag{5}$$

where $w_{i,t}$ is a binary variable that indicates the starting time point t for a hydraulic fracturing job at wellpad i.

Eq. (6) is a backward aggregation constraint from the STN model that ensures there is no overlap between different wellpad operations [46]; in other words, the only fracturing crew considered in this work cannot begin to fracture a new wellpad until he has finished fracturing the previous one.

$$\sum_{i} \sum_{t=t-Franch,-TD+1}^{t} w_{i,tt} \le 1 \qquad \forall t$$
 (6)

where $FracD_i$ represents the duration of the hydraulic fracturing operation for wellpad i, and TD represents the transition time required for moving the fracturing crew from wellpad i to the next one. Note that in Section 2, it was assumed that the completion rate and fracturing duration for each wellpad, and the transition time are given parameters.

Similarly, Eq. (7) ensures that if wellpad i is determined to be fractured, it should be completed by the end of the considered scheduling horizon (i.e., $t = t^{final}$); also, it is required that there should be at least one time period of shale gas production from this wellpad i within the scheduling horizon.

$$\sum_{t=t-FracD_t-OD_t+1}^{t} w_{i,tt} = 0 \qquad \forall i, \forall t = t^{final}$$
 (7)

where OD_i represents the time required before a steady flow of shale gas can be produced, which is also assumed as a given parameter in Section 2.

Freshwater Demand and Mass Balances in Freshwater Impoundments

Since wastewater reuse is not considered in this study, the fracturing fluid required for hydraulic fracturing operations at each wellpad can only be supplied by water withdrawal from considered freshwater sources. Thus, the demand of freshwater for all the operations at wellpad i in each time period t is described in Eq. (8).

$$fwd_{i,t} = \sum_{t=t-FracD_i+1}^{t} w_{i,t}fw_i^{wellpad} \qquad \forall i, \forall t$$
(8)

where $fw_i^{wellpad}$ is the total amount of freshwater required for wellpad i in each week. Since the completion rate of the fracturing crew is assumed as a constant, the freshwater requirements for the operations at wellpad i during each week are actually the same.

Eqs. (9)-(12) indicate that the freshwater must be pumped and stored in the impoundment installed at each wellpad in advance so that the water available at wellpad i in time period t is equal to the water demand for hydraulic operations. Specifically, as presented in Eqs. (9) and (10), the level of the impoundment in each time period ($storefw_{i,t}$) depends on the water stored in the previous time period ($storefw_{i,t-1}$), the mass flowrates of inlet streams belonging to impoundment at wellpad i

 $(pump_{f,i,t})$, and the mass flowrates of the outlet streams belonging to impoundment at wellpad i ($fwd_{i,t-1}$). At the end of the scheduling horizon, it is required that there should be no water left in impoundment, as indicated by Eq. (11). In addition, Eq. (12) guarantees that the water available in impoundment at each wellpad when the wells are going to be fractured must be greater than or equal to the water demand. Note that since there is at most one freshwater impoundment constructed at each wellpad, it is simplified to be represented by the set i.

$$0 + \sum_{f} pump_{f,i,t} = storefw_{i,t} \forall i, \forall t = 1$$
(9)

$$storefw_{i,t-1} + \sum_{f} pump_{f,i,t} - fwd_{i,t-1} = storefw_{i,t} \qquad \forall i, \forall t > 1$$
 (10)

$$storefw_{i,t} = 0 \qquad \forall i, \forall t = t^{final}$$
 (11)

$$storefw_{i,t} \ge fwd_{i,t} \qquad \forall i, \forall t$$
 (12)

The impoundment capacity (vfw_i) and the amount of water stored in the impoundment $(storefw_{i,t})$ are bounded by the maximum (SCP^{max}) capacity allowed, as indicated by Eqs. (13) and (14). The binary variables ys_i and $ysu_{i,t}$ indicate whether the freshwater impoundment is constructed at wellpad i and whether the freshwater impoundment at wellpad i is used in time period t, respectively. Eqs. (15) and (16) ensure that only the constructed impoundments can be used.

$$storefw_{i,t} \le v f w_i \qquad \forall i, \forall t$$
 (13)

$$vfw_i \le SCP^{max}ys_i \qquad \forall i \tag{14}$$

$$storefw_{i,t} \le SCP^{max}ysu_{i,t} \qquad \forall i, \forall t$$
 (15)

$$ysu_{i,t} \le ys_i \qquad \forall i, \forall t$$
 (16)

Since it was assumed in Section 2 that all the freshwater sources considered are interruptible, Eq. (17) is added to indicate that the water withdrawal from the freshwater source should be limited by its water availability.

$$\sum_{i} pump_{f,i,t} \le avail_{f,t} \qquad \forall f, \forall t$$
 (17)

where $avail_{f,t}$ is the water availability in freshwater source f in time period t.

Shale Gas Production and Mass Balances in Underground Reservoirs Similar to Eq. (8), Eq. (18) indicates the shale gas production rate at wellpad i, which defines the shale gas production profile over the scheduling horizon (sgp_{it}).

$$sgp_{i,t} = \sum_{u=1}^{t} \sum_{tt \in t-u-FracD_{t}} w_{i,tt} sg_{i,ttt}^{wellpad} \qquad \forall i, \forall t$$
 (18)

where $sg_{i,t}^{wellpad}$ is the total shale gas production rate at wellpad i in time period t.

As illustrated in Fig. 2, the extracted shale gas can be sold directly for profit; or, it can also be temporarily injected into the underground reservoir for the purpose of storage, which will undergo withdrawal and be sold in the future, as described in Eq. (19).

$$sgp_{i,t} = sgsell_{i,t} + \sum_{i} sginj_{i,r,t} \quad \forall i, \forall t$$
 (19)

where $\mathit{sgsell}_{i,t}$ is the amount of gas production at wellpad ithat is directly sold to the market in time period t, while $\mathit{sginj}_{i,r,t}$ is the amount of gas production at wellpad i that is injected into underground reservoir r in time period t.

Similar to the freshwater impoundments, the level of the underground reservoir ($storesg_{r,t}$) is represented by Eqs. (20)-(24), which is bounded by the maximum capacity (RCP_r^{max}) allowed. Note that it is also

required that there should be no gas left in the underground reservoirs at the end of the scheduling horizon, as indicated by Eq. (23).

$$injection_{r,t} = \sum_{i} sginj_{i,r,t} \quad \forall r, \forall t$$
 (20)

$$0 + injection_{r,t} = storesg_{r,t} + withdrawal_{r,t} \qquad \forall r, \forall t = 1$$
 (21)

$$storesg_{r,t-1} + injection_{r,t} = storesg_{r,t} + withdrawal_{r,t} \quad \forall r, \forall t > 1$$
 (22)

$$storesg_{r,t} = 0 \quad \forall r, \forall t = end$$
 (23)

$$storesg_{r,t} \le RCP_r^{max} \quad \forall r, \forall t$$
 (24)

where $injection_{r,t}$ represents the total amount of gas production injected into underground reservoir r in time period t, and $withdrawal_{r,t}$ represents the total amount of gas production withdrawn from underground reservoir r in time period t.

Thus, the total amount of shale gas production sold in time period t ($output_t$) is calculated, which consists of the total amount of gas production directly sold in time period t ($output1_t$) and the total amount of gas production withdrawn from the underground reservoirs in time period t ($output2_t$). It should be bounded by the minimum ($Demand_t^{min}$) and maximum ($Demand_t^{max}$) (predicted) production demand.

$$output1_{t} = \sum_{i} sgsell_{i,t} \qquad \forall t$$
 (25)

$$output2_t = \sum_{r} withdrawal_{r,t} \quad \forall t$$
 (26)

$$output_t = output1_t + output2_t \quad \forall t$$
 (27)

$$Demand_{t}^{min} \leq output_{t} \leq Demand_{t}^{max} \quad \forall t$$
 (28)

3.2.2. Constraints at control level

According to Section 3.1, a ROM is developed to represent the process dynamics and integrated with the scheduling level. In this study, a 3rd-order linear time-invariant state-space model is used. Thus, the following constraints are added as Eqs. (29) and (30).

$$\begin{bmatrix} x_{1} \\ x_{2} \\ x_{3} \end{bmatrix}_{i,st,k+1} = \begin{bmatrix} A_{11} & A_{12} & A_{13} \\ A_{21} & A_{22} & A_{23} \\ A_{31} & A_{32} & A_{33} \end{bmatrix} \begin{bmatrix} x_{1} \\ x_{2} \\ x_{3} \end{bmatrix}_{i,st,k} + \begin{bmatrix} B_{11} & B_{12} \\ B_{21} & B_{22} \\ B_{31} & B_{32} \end{bmatrix} \begin{bmatrix} u_{1} \\ u_{2} \end{bmatrix}_{i,st} \quad \forall i, \forall st, \forall k$$
(29)

$$\begin{bmatrix} y_1 \\ y_2 \\ y_3 \end{bmatrix}_{i,st,k} = \begin{bmatrix} C_{11} & C_{12} & C_{13} \\ C_{21} & C_{22} & C_{23} \\ C_{31} & C_{32} & C_{33} \end{bmatrix} \begin{bmatrix} x_1 \\ x_2 \\ x_3 \end{bmatrix}_{i,st,k} \quad \forall i, \forall st, \forall k$$
 (30)

where $x_{i,st,k}$ represents the three system states (i.e., x_1, x_2, x_3 with no physical meanings) in pumping stage st and at time step k at wellpad i, $u_{i,st}$ represents the two inputs (i.e., the flowrate, $q_{i,st}$, and proppant concentration, $c_{i,st}$, of the injected hydraulic fracturing fluid) in pumping stage st at wellpad i, $y_{i,st,k}$ represents the three outputs (i.e., the average fracture width, $W_{i,st,k}^{avg}$, fracture width at the wellbore, $W_{i,st,k}^{wellbore}$, and fracture length, $L_{i,st,k}$) in pumping stage st and at time step k at wellpad t. Note that the total number of time steps in each pumping stage depends on the duration of each pumping stage and the simulation step considered when generating the ROM. In this study, the duration of each pumping stage is 500 s, and the simulation step is 0.3 s; thus, the total number of time steps considered in this study is 1667. Hence, the initial state of the current pumping stage ($x_{i,st-1,k=1667}$), as indicated in Eq. (31).

$$\begin{bmatrix} x_1 \\ x_2 \\ x_3 \end{bmatrix}_{i,y,k=1} = \begin{bmatrix} x_1 \\ x_2 \\ x_3 \end{bmatrix}_{i,y-1} \forall i, \forall st$$
 (31)

In general, the proppant concentration of the injected hydraulic fracturing fluid should be increased monotonically; in addition, a minimum increment of 0.002 is considered in this study, as shown in Eq. (32). As described in Eqs. (33) and (34), the flowrate and proppant concentration of the injected hydraulic fracturing fluid should be within the reasonable ranges for operability (i.e., FWQ^{min} and FWQ^{max} for flowrate, and $PropC^{min}$ and $PropC^{min}$ for proppant concentration).

$$c_{i,st+1} = c_{i,st} + 0.002 \qquad \forall i, \forall st \tag{32}$$

$$FWQ^{min} \le q_{i,st} \le FWQ^{max} \qquad \forall i, \forall st$$
 (33)

$$PropC^{min} \le c_{i,st} \le PropC^{max} \quad \forall i, \forall st$$
 (34)

With the average fracture width at the end of pumping, the propped fracture width at the end of the closure can be approximated as indicated by Eq. (35). Then, Eq. (36) is used to calculate the propped fracture length, as explained in Section 3.1.

$$(1 - \phi)W_{i \text{ of } -9 \text{ } k-1667}^{avg} = \alpha W_{i}^{propped} \qquad \forall i$$
(35)

$$L_i^{propped} = prop_i^{fracture} / \left(2\rho_{sd} h_{eq} (1 - \phi) W_{i,st=9,k=1667}^{avg} \right) \qquad \forall i$$
 (36)

where $W_i^{propped}$ and $L_i^{propped}$ represent the average propped fracture width and propped fracture length of the fracture at wellpad i, respectively. $prop_i^{fracture}$ is the amount of proppant required for the hydraulic fracturing operation to stimulate a single fracture.

3.2.3. Constraints that link scheduling and control levels

The linking variables for the scheduling and control levels are the freshwater requirement and shale gas production. Specifically, the amount of freshwater required to stimulate a fracture at wellpad i ($fw_i^{fracture}$) can be calculated based on the designed pumping profile, as indicated in Eq. (37) [2].

$$f_{w_{i}}^{fracture} = 2(F_0 + \sum_{st} q_{i,st} (1 - c_{i,st}) T_{stage}) \qquad \forall i$$
 (37)

where F_0 is the amount of freshwater consumed during pad time, and T_{stage} is the duration of each pumping stage. Note that the pad time and pumping stage duration are fixed parameters. Additionally, since the number of fractures per stage (N_i) and completion rate (R_i) for wellpad i are assumed as parameters in Section 2, the total amount of freshwater required for wellpad i in each time period can be computed by Eq. (38).

$$fw_i^{wellpad} = 2(F_0 + \sum_{st} q_{i,st} (1 - c_{i,st}) T_{stage}) N_i R_i \qquad \forall i$$
(38)

Similarly, Eqs. (39) and (40) describe the amount of proppant required to stimulate a fracture at wellpad i ($prop_i^{fracture}$) and the total amount of proppant required to complete wellpad i ($prop_i^{wellpad}$) as follows.

$$prop_{i}^{fracture} = 2\left(\sum_{st} \rho_{sd} q_{i,st} c_{i,st} T_{stage}\right) \quad \forall i$$
 (39)

$$prop_{i}^{wellpad} = 2 \left(\sum_{st} \rho_{sd} q_{i,st} c_{i,st} T_{stage} \right) N_{i} R_{i} Frac D_{i} \qquad \forall i$$
(40)

On the other hand, based on the maps generated from CMG simulations in Section 3.1 (i.e., represented using functions f and g, respectively), the cumulative shale gas production of one year ($cumsg_i^{fracture}$) from one fracture, and the corresponding shale gas production profile

 $(sg_{i,t}^{fracture})$ from one fracture at wellpad i can be calculated based on propped fracture geometry $(L_i^{propped}, W_i^{propped})$ as shown in Eqs (41) and (42).

$$cumsg_i^{fracture} = 2f(L_i^{propped}, W_i^{propped}) \qquad \forall i$$
 (41)

$$sg_{i,t}^{fracture} = cumsg_i^{fracture}g(t) \qquad \forall i, \forall t$$
 (42)

Also, the shale gas production profile from all the fractures at well-pad i can be calculated as follows.

$$sg_{i,t}^{wellpad} = cumsg_i^{fracture}g(t)N_iR_iFracD_i \qquad \forall i, \forall t$$
 (43)

3.2.4. Objective

The objective function, which is to be maximized, comprises the revenue (from selling the gas production) and the costs (from drilling and production, freshwater and propant acquisition, freshwater impoundment construction and use, and underground reservoir use) as described in Eq. (44). Note that transportation cost is not considered in this study, as assumed in Section 2.

$$Profit = Revenue^{sas} - Cost^{drill} - Cost^{fw} - Cost^{prop} - Cost^{storefw} - Cost^{storesg}$$
(44)

Herein, the cost for drilling, completion, and production (*Cost*^{drill}) is defined by Eq. (45).

$$Cost^{drill} = \sum_{i} \sum_{t} C_{i}^{drill} w_{i,t} + \sum_{i} \sum_{t} C_{i}^{prod} sgp_{i,t}$$

$$\tag{45}$$

where C_i^{drill} is the drilling cost and C_i^{prod} is the unit shale gas production cost.

Freshwater cost $(Cost^{fw})$ includes the pumping cost from the freshwater sources, while proppant cost $(Cost^{prop})$ includes the acquisition cost from the market, which are described in Eqs. (46) and (47). Note that y_i^{well} is required in Eq. (47), which represents whether the wellpad i is fracked within the scheduling horizon. Since there is no binary variable used to formulate the constraints for flowrate $(q_{i,st})$ and proppant concentration $(c_{i,st})$, $prop_i^{wellpad}$ should always be nonzero as computed by Eq. (40). To assure that only the proppant costs from the fracked wellpads are included in the objective function, Eq. (48) is added.

$$Cost^{fw} = \sum_{f} \sum_{i} \sum_{t} C_{f}^{pump} pump_{f,i,t}$$
(46)

$$Cost^{prop} = \sum_{i} C^{propac} prop_{i}^{wellpad} y_{i}^{well}$$
(47)

$$y_i^{well} = \sum w_{i,i} \qquad \forall i \tag{48}$$

where C_f^{pump} is the water withdrawal cost and C^{propac} is the proppant acquisition cost.

Impoundments should be constructed at the wellpad by the operator if it is going to be fracked. Thus, the related cost for each impoundment consists of the base investment cost, incremental cost based on the designed capacity of the impoundment, and the operating cost for use, as described in Eq. (49).

$$Cost^{storefw} = \sum_{i} (C^{sto_base} y s_i + C^{sto_incre} v f w_i) + \sum_{i} C^{sto_oper} y s u_{i,t}$$
 (49)

where $Cost^{storefw}$ is the total impoundment cost, C^{sto_base} is the base investment cost required to construct an impoundment, C^{sto_incre} is the unit incremental investment cost for impoundment, and C^{sto_oper} is the unit operating cost for impoundment.

The cost related to underground reservoir (*Cost*^{storesg}) includes the injection cost and withdrawal cost, as shown in Eq. (50).

$$Cost^{storesg} = \sum_{r} \sum_{l} C_{r}^{injection} injection_{r,l} + C_{r}^{withdrawal} withdrawal_{r,l}$$
 (50)

where $C_r^{injection}$ and $C_r^{withdrawal}$ are the unit injection cost and unit withdrawal cost at underground reservoir, respectively.

The revenues of shale-gas sales ($Revenue_1^{gas}$) within the scheduling horizon can be represented by Eq. (51).

$$Revenue_1^{gas} = \sum_{t} R_t^{gas1} output_t$$
 (51)

where R_t^{sas1} is the forecast of gas price in time period t. Considering that the lifetime of a shale well is typically more than a decade, the revenue of shale gas produced after the considered scheduling horizon is also approximated and added to the objective function. Specifically, based on Eq. (43), the shale gas production profile at wellpad i for a T-year horizon $(sg_{i,T}^{wellpad})$ can be computed in a similar manner. Thus, for the first T years of production period of wellpad i, the total amount of shale gas produced out of the scheduling horizon $(adtotalsg_i^{wellpad})$ could be obtained by Eq. (52).

$$adtotalsg_{i}^{wellpad} = \sum_{T} sg_{i,T}^{wellpad} y_{i}^{well} - \sum_{T} sgp_{i,t}$$
 (52)

Thus, the revenues of shale-gas sales out of the scheduling horizon can be roughly approximated by Eq. (53). Note that the gas price (R^{gas2}) is assumed as constant and slightly lower than the lowest R_t^{gas1} within the scheduling horizon.

$$Revenue_2^{gas} = \sum_{i} R^{gas2} adtotals g_i^{wellpad}$$
 (53)

With the revenues of shale gas production defined in Eqs. (51) and (53), the total revenue obtained from selling the gas production can be represented by Eq. (54).

$$Revenue_1^{gas} = Revenue_1^{gas} + Revenue_2^{gas}$$
 (54)

Consequently, combining the objective functions (Eqs. (44)-(54)), the constraints at both the scheduling level (Eqs. (5)-(28)) and control level (Eqs. (29)-(36)), and the linking constraints (Eqs. (37)-(43)), the optimization model for the integrated problem in the outer loop of the proposed framework can be obtained.

3.3. Offset-free MPC control system

According to the proposed online integrated framework, the output reference trajectories are determined by solving the integrated scheduling and control model in the outer loop where the ROM is employed to represent the process dynamics. The same ROM is also used in the MPC control system in the inner loop whose objective is to track the output references. However, since the ROM is mainly developed based on limited simulation data, it cannot completely represent the complex dynamics of the hydraulic fracturing process; in other words, the prediction error may always exist due to the plant-model mismatch. In this sense, the offset-free MPC scheme is necessary to remove the undesirable performance degradation induced by the plant-model mismatch [44]. Hence, based on the developed ROM as shown in Eqs. (1) and (2) in Section 3.1, the nominal model is augmented with a disturbance model as follows:

$$x(t_{k+1}) = Ax(t_k) + Bu(t_k) + B_d d(t_k)$$
(55)

$$y(t_k) = Cx(t_k) + C_d d(t_k)$$
(56)

$$d(t_{k+1}) = d(t_k) \tag{57}$$

where d is the disturbance vector, and B_d and C_d are disturbance model matrices denoting the influence of disturbance on the evolution of state and output, respectively.

Here, it is free to choose how the integrated disturbance affects the state and output variables through the choice of B_d and C_d , and the only restriction is that the augmented system is detectable. To ensure the observability of the augmented system in Eqs. (55)-(57), (A, C) should be observable, and the chosen B_d and C_d should satisfy the constraints as shown in Eq. (58):

$$rank \begin{bmatrix} I - A & -B_d \\ C & C_d \end{bmatrix} = n_x + n_d \tag{58}$$

where n_x is the dimension of the state, and n_d is the dimension of the disturbance. Note that according to the offset-fee control theory, n_d is chosen to be 2 in this study, which is the number of measurements in the hydraulic fracturing operation [44].

On the other hand, as mentioned in Section 3.1, the unmeasurable average fracture width needs to be estimated through a Kalman filter. Thus, a Kalman filter is developed based on the obtained ROM and the available measurements as shown in Eqs. (59)-(61):

$$\widehat{x}(t_{k+1}) = A\widehat{x}(t_k) + Bu(t_k) + M(t_k)[y_m(t_k) - \widehat{y}(t_k)]$$
(59)

$$M(t_k) = P(t_k)C^T [R(t_k) + CP(t_k)C^T]^{-1}$$
(60)

$$P(t_{k+1}) = [I - M(t_k)C]P(t_k)$$
(61)

where $\widehat{x}(t_k)$ and $\widehat{y}(t_k)$ are the estimates of the state and output variables, respectively, $M(t_k)$ is the Kalman filter gain, and $P(t_k)$ is the covariance of the state estimation error. The Kalman filter allows the state estimates to be updated iteratively based on the available real-time measurements.

Similarly, with the proper B_d and C_d that satisfy Eq. (58), the following state and disturbance estimators can be designed based on Kalman filter. In detail, Kalman filter is a two-step process including measurement update and prediction. Thus, the state and the disturbance are estimated by Eqs. (62) and (63) as follows:

$$\begin{bmatrix} \widehat{x}(t_k|t_k) \\ \widehat{d}(t_k|t_k) \end{bmatrix} = \begin{bmatrix} \widehat{x}(t_k|t_{k-1}) \\ \widehat{d}(t_k|t_{k-1}) \end{bmatrix} + \begin{bmatrix} L_x(t_k) \\ L_d(t_k) \end{bmatrix} \left(y_m(t_k) - C\widehat{x}(t_k|t_{k-1}) - C_d\widehat{d}(t_k|t_{k-1}) \right)$$
(62)

$$\widehat{y}(t_k|t_k) = \begin{bmatrix} C & C_d \end{bmatrix} \begin{bmatrix} \widehat{x}(t_k|t_k) \\ \widehat{d}(t_k|t_k) \end{bmatrix}$$
(63)

Subsequently, the prediction of the future augmented state is obtained by Eq. (64).

$$\begin{bmatrix} \widehat{x}(t_{k+1}|t_k) \\ \widehat{d}(t_{k+1}|t_k) \end{bmatrix} = \begin{bmatrix} A & B_d \\ 0 & I \end{bmatrix} \begin{bmatrix} \widehat{x}(t_k|t_k) \\ \widehat{d}(t_k|t_k) \end{bmatrix} + \begin{bmatrix} B \\ 0 \end{bmatrix} u_k$$
 (64)

where $L_x(t_k)$ and $L_d(t_k)$ are the filter gain matrices for the state and the disturbance, respectively, \hat{x} is the estimated state, \hat{d} is the estimated disturbance, and y_m is the measurement from the process, including $W^{wellbore}$ and L. Then, Eqs. (62) and (64) can be integrated into one step as shown in Eq. (65), which is similar to Eq. (59).

Thus, by manipulating the flowrate and proppant concentration of the injected hydraulic fracturing fluid, an offset-free MPC control system is formulated with the objective to minimize the squared deviation of the actual fracture geometry (i.e., only the average fracture width is the controlled variable) from its reference value (i.e., obtained from solving the integrated problem as described in Section 3.2) during the entire hydraulic fracturing process, which is presented in Eqs. (67)-(75).

$$\min_{\substack{C_{\textit{Starge-8}}, \cdots, C_{\textit{Starge-9}}\\ \mathcal{Q}_{\textit{Starge-9}}}} J = \sum\nolimits_{i=k}^9 \left(\widehat{y}(t_{i+1}) - r_y(t_{i+1})\right)^T \mathcal{Q}_c\left(\widehat{y}(t_{i+1}) - r_y(t_{i+1})\right) + \mathcal{Q}_\varepsilon \varepsilon^2$$

s.t.
$$\widehat{x}(t_k) = x(t_k); \ \widehat{d}(t_k) = d(t_k)$$
 (68)

(67)

$$x(t_{k+1}) = Ax(t_k) + Bu(t_k) + B_d d(t_k)$$
(69)

$$y(t_k) = Cx(t_k) + C_d d(t_k)$$
(70)

$$Q_{min} \le Q_{stage,k} \le Q_{max} \tag{71}$$

$$C_{stage,k-1+m} \le C_{stage,k+m} - 0.002$$
 (72)

$$m = 1, \dots 9 - k; \ \varepsilon \ge 0 \tag{73}$$

$$\Delta \left(\sum_{k=1}^{9} 2Q_{stage,k} \left(1 - C_{stage,k} \right) \right) \le f w_i^{fracture} / 2$$
 (74)

$$prop_{i}^{fracture} / 2 - \varepsilon \le \Delta \left(\sum_{k=1}^{9} 2Q_{stage,k} C_{stage,k} \right) \le prop_{i}^{fracture} / 2 + \varepsilon$$
 (75)

where r_y is the output reference obtained from the integrated problem, Δ is the sampling time, t_k is the current time, $Q_{stage,k}$ and $C_{stage,k}$ are the flowrate and proppant concentration of injected hydraulic fracturing fluid at k^{th} pumping stage (i.e., $[t_k, t_k + \Delta)$), which should be computed online by solving the control problem. The objective function in Eq. (67) describes the squared deviation of the output variables utilizing the weight matrix Q_c and the squared value of the slack variable utilizing the weight matrix Q_{ϵ} . The aforementioned Kalman filter is included in this control system to estimate the augmented state variable and the unmeasurable average fracture width. Note that the Kalman filter is initialized at every sampling time t_k as described in Eq. (68), utilizing the available measurements of the fracture width at the wellbore and the fracture length at the k^{th} sampling time (i.e., $W_0(t_k)$ and $L(t_k)$). The augmented model is represented using Eqs. (69) and (70). The operational constraint in Eq. (71) imposes the limits on the injection flowrate while Eq. (72) implies that the proppant concentration will be increased monotonically where a minimum gap of 0.002 is added in this study. Eqs. (74) and (75) are mainly used to calculate the amount of freshwater and proppant consumption; the former is required to be equal to or less than the designed freshwater requirement from the integrated problem,

$$\begin{bmatrix}
\widehat{x}(t_{k+1}|t_{k+1}) \\
\widehat{d}(t_{k+1}|t_{k+1})
\end{bmatrix} = \begin{bmatrix} A & B_d \\
0 & I \end{bmatrix} \begin{bmatrix} \widehat{x}(t_k|t_k) \\
\widehat{d}(t_k|t_k) \end{bmatrix} + \begin{bmatrix} B \\
0 \end{bmatrix} u(t_k) + \begin{bmatrix} L_x(t_{k+1}) \\
L_d(t_{k+1}) \end{bmatrix} \begin{pmatrix} y_m(t_{k+1}) - [C & C_d] \begin{bmatrix} \widehat{x}(t_{k+1}|t_k) \\
\widehat{d}(t_{k+1}|t_k) \end{bmatrix} \end{pmatrix}$$
(65)

where $L_1(t_k)$ and $L_2(t_k)$ are the predictor gain matrices for the state and the disturbance, respectively, which satisfy Eq. (66).

$$\begin{bmatrix} L_1(t_k) \\ L_2(t_k) \end{bmatrix} = \begin{bmatrix} A & B_d \\ 0 & I \end{bmatrix} \begin{bmatrix} L_x(t_k) \\ L_d(t_k) \end{bmatrix}$$
(66)

and the latter is required to be exactly the same as the designed value. In particular, a nonnegative slack variable ε is introduced to Eq. (75) to assure the feasibility of the designed control system. Note that a control system is designed for a specific wellpad; in other words, the number of control systems should be equal to the number of wellpads to be fracked.

3.4. Re-solving the integrated scheduling and control model online

According to the proposed online implementation strategy, resolving the integrated scheduling and control model based on feedback information is only for the wellpads that have not been fracked. In this sense, the considered scheduling horizon can be essentially divided into two sub-horizons: (1) the historical horizon, and (2) the future horizon. Specifically, the integrated scheduling and control model should be re-solved in the future horizon while all the variables in the historical period should be fixed. To formulate the reduced integrated problem, the following changes have been incorporated into the original integrated model:

- The set of time periods should be reduced to only include the future horizon:
- The set of candidate wellpads should exclude the ones that have been completed;
- The freshwater impoundment storage levels at unfracked wellpads in the first time period of the future horizon should be dependent on the level in the last time period of the historical horizon;
- The underground reservoir storage level in the first time period of the future horizon should be dependent on the level in the last time period of the historical horizon;
- The actual shale gas production forecast from the completed wellpads should be introduced to the integrated model as a new parameter and added to the total shale gas production.

It is worthy to note that since the construction of an impoundment generally requires a long time period in practice and its capacity is difficult to be changed after the construction, they are determined only at the design phase and then fixed as parameters according to the offline solution, when the integrated scheduling and control problem is resolved online (i.e., the capacity of impoundments will not be updated online unlike the scheduling decisions and output references).

4. Solution strategy

For the integrated problem explained in Section 3.2, the proposed optimization model is an MINLP model. This model involves two types of bilinear terms: (1) the product of two continuous variables in calculating the amount of freshwater and proppant required for the hydraulic fracturing operations (e.g., Eqs. (37) and (39)) and the propped fracture geometry (e.g., Eq. (36)); and (2) the product of a binary and a continuous variable in calculating the freshwater demand and shale gas production over the scheduling horizon (e.g., Eqs. (8) and (18)). Thus, to solve the aforementioned MINLP problem, a solution strategy that utilizes the following techniques is implemented in this study.

First, the bilinear term of hydraulic fracturing fluid injection flowrate multiplied by proppant concentration is relaxed using under and over estimators (i.e., McCormick convex envelope [3]), which is thus replaced using a single continuous variable $M_{i,st}$. To this end, the following equations are added as additional constraints (Eqs. (76)-(79)).

$$q_{i,st}c_{i,st} = M_{i,st} \ge FWQ^{min}c_{i,st} + PropC^{min}q_{i,st} - FWQ^{min}PropC^{min}$$
(76)

$$q_{i,st}c_{i,st} = M_{i,st} \ge FWQ^{max}c_{i,st} + PropC^{max}q_{i,st} - FWQ^{max}PropC^{max}$$
(77)

$$q_{i,st}c_{i,st} = M_{i,st} \le FWQ^{max}c_{i,st} + PropC^{min}q_{i,st} - FWQ^{max}PropC^{min}$$
(78)

$$q_{i,st}c_{i,st} = M_{i,st} \le FWQ^{min}c_{i,st} + PropC^{max}q_{i,st} - FWQ^{min}PropC^{max}$$
(79)

On the other hand, the bilinear term of propped fracture length multiplied by average propped fracture width is approximated using another strategy. One particular reason for this consideration is that there are no constraints specified for the propped fracture geometry. In this case, we discretize propped fracture length and disaggregate the average propped fracture width for approximation, as shown in Eqs.

(80)-(83).

$$L_i^{prop} = \sum_{l} Leng_l z_{i,l} \qquad \forall i$$
 (80)

$$\sum_{l} z_{i,l} = 1 \qquad \forall i \tag{81}$$

$$Wid_{i,l} = \frac{(1-\phi)W_{i,st=9,k=1667}^{avg}}{\alpha} z_{i,l} \qquad \forall i, \forall l$$
(82)

$$W_{i}^{prop} = \sum_{i} Wid_{i,l} \qquad \forall i$$
 (83)

where $z_{i,l}$ is the binary variable selecting only one length value $Leng_l$ (i.e., parameter) to represent the variable L_i^{prop} , and $Wid_{i,l}$ is the disaggregated variable for W_i^{prop} . Note that in Eq. (82), $W_{i,st=9,k=1667}^{org} z_{i,l}$ is also a bilinear term (i.e., the product of a binary and continuous variable), which will be further linearized using the strategy explained below. In this sense, the bilinear term can be linearized as indicated in Eq. (84).

$$W_{i}^{prop}L_{i}^{prop} = \sum_{l}Wid_{i,l}Leng_{l} \qquad \forall i$$
 (84)

Finally, the product of a binary and a continuous variable can be linearized by using a Big-M formulation. Taking Eq. (8) as an example, the bilinear term $w_{i,t}fw_i^{wellpad}$ is replaced by the intermediate continuous variable $Xfw_{i,t}$, and Eqs. (86)–(88) are added as necessary constraints for this linearization.

$$w_{i,t} f w_i^{wellpad} = X f w_{i,t} \qquad \forall i, \forall t$$
 (85)

$$X f w_{i,t} \le f w_i^{wellpad} \qquad \forall i, \forall t$$
 (86)

$$Xfw_{i,t} \le w_{i,t}BM \qquad \forall i, \forall t$$
 (87)

$$Xf w_{i,t} > f w_i^{wellpad} - (1 - w_{i,t}) BM \qquad \forall i, \forall t$$
 (88)

where BM must be greater than or equal to $fw_i^{wellpad}$. Generally, the upper bound of $fw_i^{wellpad}$ is used in the equation; BM can be used for the case where the upper bound is unknown.

With the three techniques mentioned above, the original MINLP problem can be relaxed, which leads to an MILP problem. Then, the binary variables obtained by solving the relaxed MILP problem, which represent the fracturing schedule, are fixed as parameters into the original MINLP. Lastly, the resulting smaller MINLP problem is solved to get the final optimal solution.

The mathematical model is implemented in GAMS 27.1. The relaxed MILP problem is solved with CPLEX 12.9, and the MINLP problem with a fixed fracturing schedule is solved with DICOPT 2 using CONOPT4 to solve the NLP subproblems, and CPLEX 12.9 to solve the MIP subproblems. Note that DICOPT is a local solver, and thus, the global solution cannot be guaranteed; however, the final solution is shown to be better than the one obtained from solving the original MINLP problem directly.

5. Results and discussion

In this section, the effectiveness of the proposed online integrated framework has been demonstrated by applying it to a hypothetical case study designed based on Marcellus Shale Play, where the development of a set of wellpads in a relatively small area is considered. First, the performances of the developed ROM and Kalman filter are presented. Also, the shale gas production prediction based on the CMG-GEM software and the maps necessary for designing the integrated model are presented. Next, the details of the case study and the optimal solutions obtained from solving the integrated problem offline (in the design phase before the online implementation) are discussed. Then, the online control solutions from the designed offset-free MPC system are given.

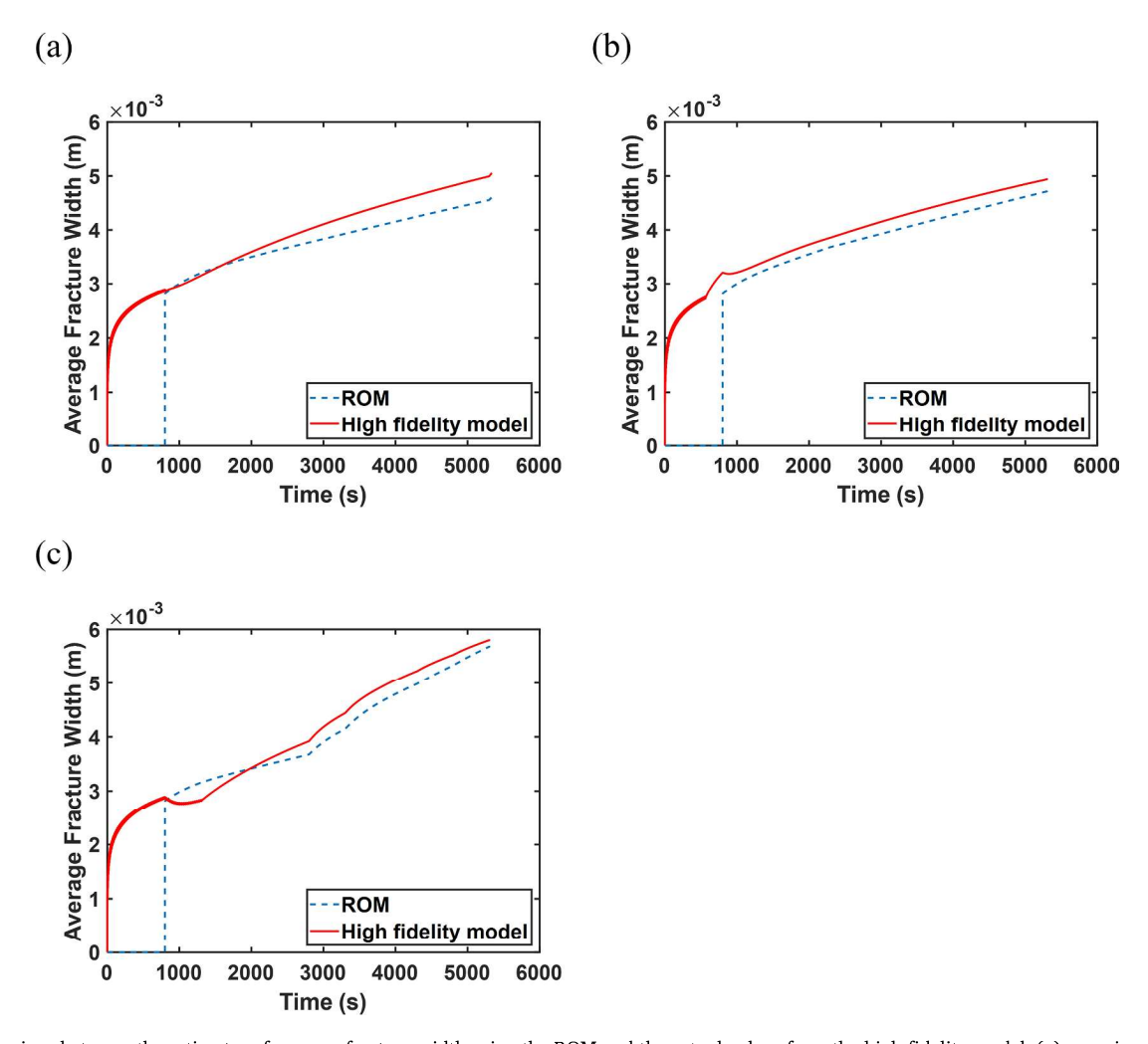


Fig. 6. Comparison between the estimates of average fracture width using the ROM and the actual values from the high-fidelity model. (a) pumping profile 1, with which the resulting propped fracture half-length is 120 m, (b) pumping profile 2, with which the resulting propped fracture half-length is 94.5 m, and (c) pumping profile 3, with which the resulting propped fracture half-length is 153 m.

Finally, the complete results from the proposed closed-loop integrated framework are provided and compared with the ones from the openloop optimization.

$5.1. \ Hydraulic\ fracturing\ modeling\ and\ shale\ gas\ production\ simulation$

By utilizing the dynamic model of the hydraulic fracturing process, the input/output simulation data can be generated from the high-fidelity model, which are subsequently used to identify a data-driven ROM. Note that the training input data is designed to consider the necessary operational constraints. As described in Section 3.2, the developed ROM is in the form of a 3rd-order linear time-invariant state-space model (Eqs. (29) and (30)), where the *A*, *B*, and *C* matrices obtained using MOESP algorithm are given in Eqs. (89)-(91).

$$A = \begin{bmatrix} 0.9996 & 1.2434 \times 10^{-4} & -2.3447 \times 10^{-4} \\ 2.0100 \times 10^{-4} & 0.9998 & 1.87187 \times 10^{-4} \\ -6.0175 \times 10^{-4} & 2.8465 \times 10^{-4} & 0.9996 \end{bmatrix}$$
(89)

$$B = \begin{bmatrix} 8.4973 \times 10^{-4} & -2.0869 \times 10^{-5} \\ -7.2948 \times 10^{-4} & 3.1820 \times 10^{-5} \\ 0.0011 & 3.6069 \times 10^{-5} \end{bmatrix}$$
(90)

$$C = \begin{bmatrix} 344.7757 & -89.6820 & 1.1178 \\ 592.6783 & 42.6837 & -0.4109 \\ 1.2885 \times 10^3 & -549.1472 & -1.7597 \times 10^3 \end{bmatrix}$$
(91)

To show the prediction capability of the ROM, different pumping profiles are used for validation. Fig. 6 presents the comparison between the average fracture width estimated by the developed ROM and the one from the high-fidelity model.

As explained in Section 3.3, a Kalman filter is designed based on the developed ROM for state and output estimation. Thus, the unmeasurable average fracture width can be estimated through the Kalman filter using the available measurements of the fracture width at the wellbore and the fracture length. Fig. 7 shows that the estimated average fracture width quickly converges to the actual value generated from the high-fidelity model (i.e., training data is used). Note that $t_p=800s$ is assumed for the pad time. Since the designed Kalman filter and offset-free MPC control system are initialized exactly at $t_p=800s$, operation during pad time is fixed and not considered in the control system.

Once the fracture geometry at the end of pumping is obtained, the corresponding propped fracture geometry can be approximated as explained in Section 3.1. Then, the propped fracture geometry, including the propped fracture length, width, and height, are used as inputs to the reservoir simulator, CMG. The other parameters necessary for shale gas production simulation are mainly taken from Mao et al. [46], which are provided in Table A1 in Appendix A. Note that the reservoir thickness is modified based on the consideration in our high-fidelity model (i.e., 60m) [2].

Utilizing the CMG reservoir simulator, the daily shale gas production rates from a half-fracture are forecasted for a period of five years.

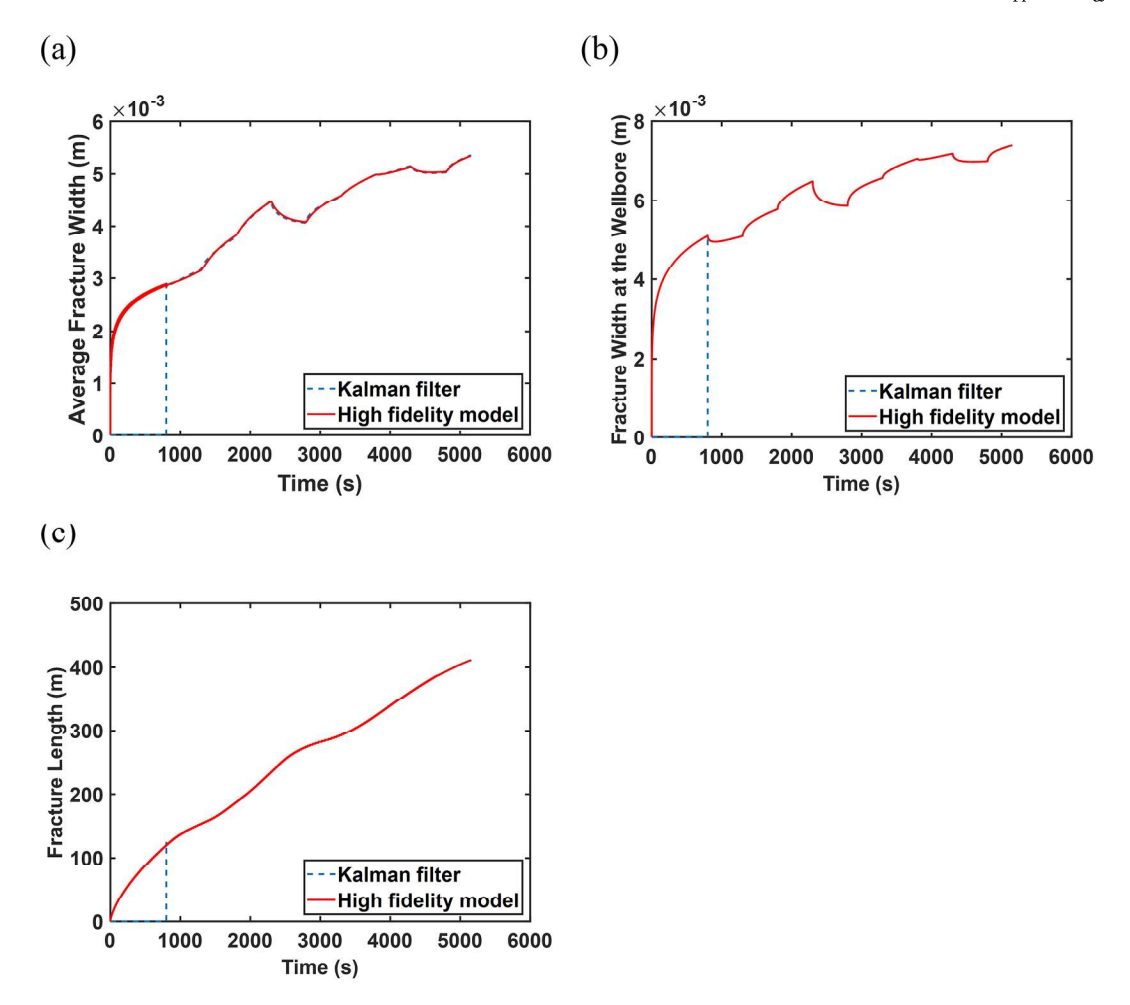


Fig. 7. Comparison between the estimates of (a) average fracture width, (b) fracture width at the wellbore, and (c) fracture length using the Kalman filter and the actual values from the high-fidelity model.

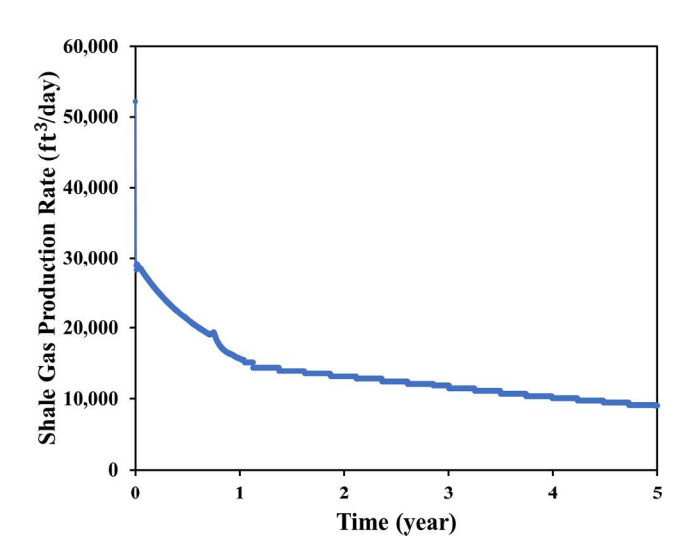


Fig. 8. Shale gas production rate (ft^3/day) for a half-fracture (propped fracture width: 0.0024m; and propped fracture half-length: 60m).

Typical production simulation results are shown in Fig. 8, which correspond to a half-fracture with its propped fracture width as 0.0024m and its propped fracture half-length as 60m.

To formulate the integrated scheduling and control model, the relationship between the propped fracture geometry and shale gas daily production rate is necessary. In this study, it is assumed that the reservoir parameters and the operating conditions are constant; thus, the shale gas production rate is mainly a function of the propped fracture geometry. Considering that the propped fracture height is assumed fixed as the equilibrium height of the formulated proppant bank, only the propped fracture width and half-length are the controlled variables. Thus, a set of widths and half-lengths are applied to the CMG software to generate the input/output simulation data. To establish the desired relationship, two maps are generated using the curve fitting function in MATLAB with the R-square values larger than 99%, which are presented in Fig. 9.

Specifically, with the first map (i.e., Fig. 9(a)), the cumulative shale gas production of one year can be approximated based on the propped fracture width and half-length; thereafter, with the second map (i.e., Fig. 9(b)), the weekly shale gas production rate can be approximated based on the corresponding cumulative shale gas production. The two maps can be described using Eqs. (92)-(93), respectively.

$$f(W^{propped}, L^{propped}) = 34320 + 2191000W^{propped} + 119700L^{propped}$$

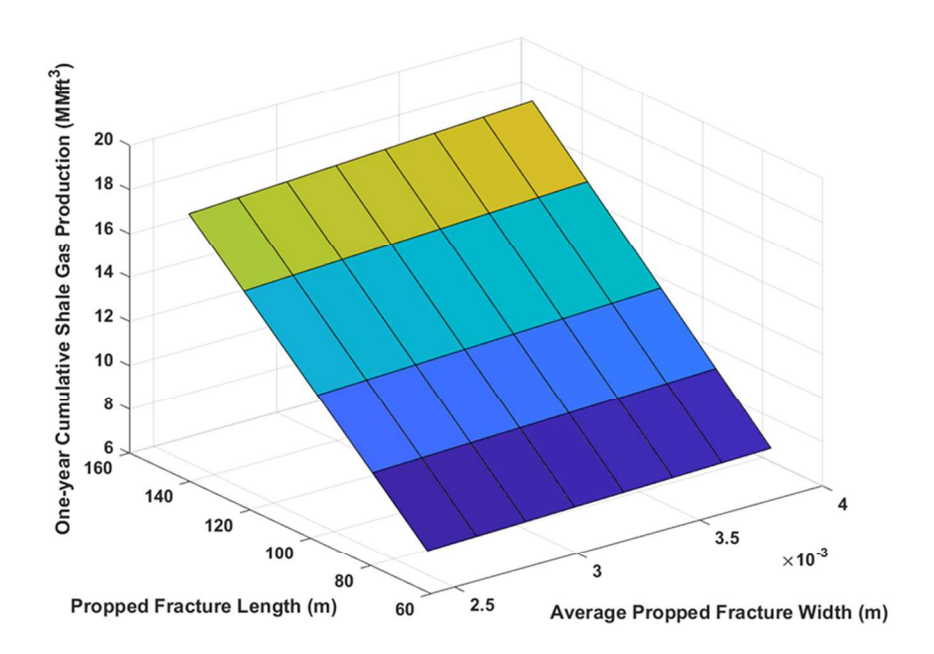
$$+4003000W^{propped}L^{propped} - 0.02102L^{propped}L^{propped}$$

$$(92)$$

$$g(t) = 0.0301 / \left(1 + 0.0841(t - 1)^{1/1.587}\right)$$
(93)

These two equations are incorporated into the integrated problem through Eqs. (41)-(42). Here, although Eq. (92) is a nonlinear equation, it can be linearized using the technique shown in Eq. (80)-(84).

(a)



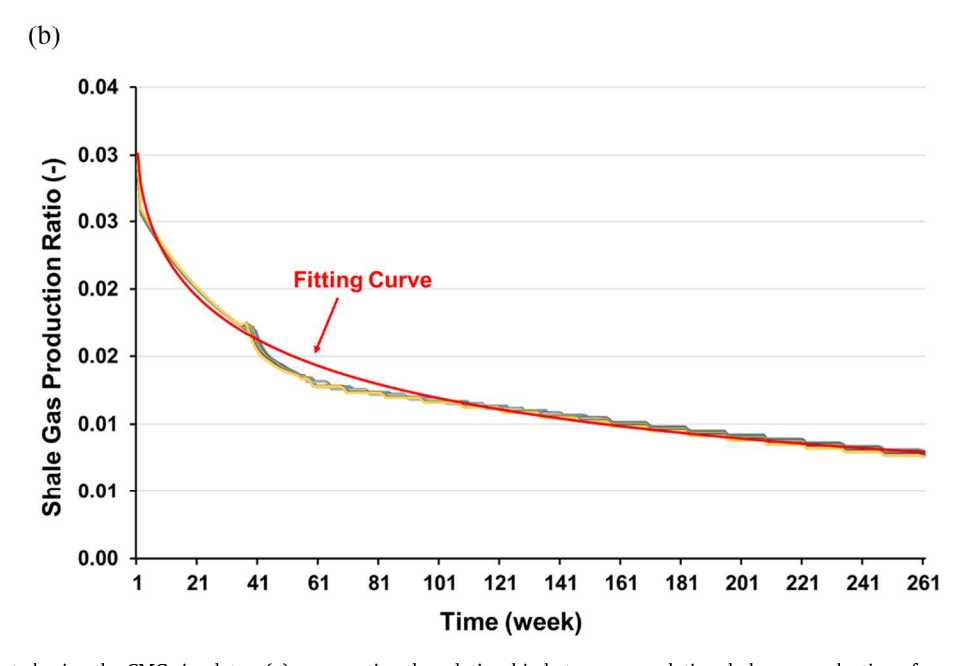


Fig. 9. Two maps generated using the CMG simulator: (a) representing the relationship between cumulative shale gas production of one year and propped fracture geometry; (b) representing the relationship between the ratio of weekly shale gas production to one-year cumulative production.

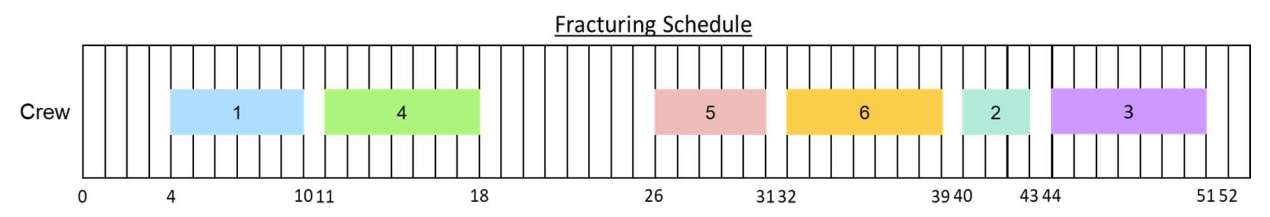


Fig. 10. Optimal fracturing schedule for the wellpads (the lengths of the colored boxes represents the operation times; the numbers within the colored boxes represent the wellpad indices).

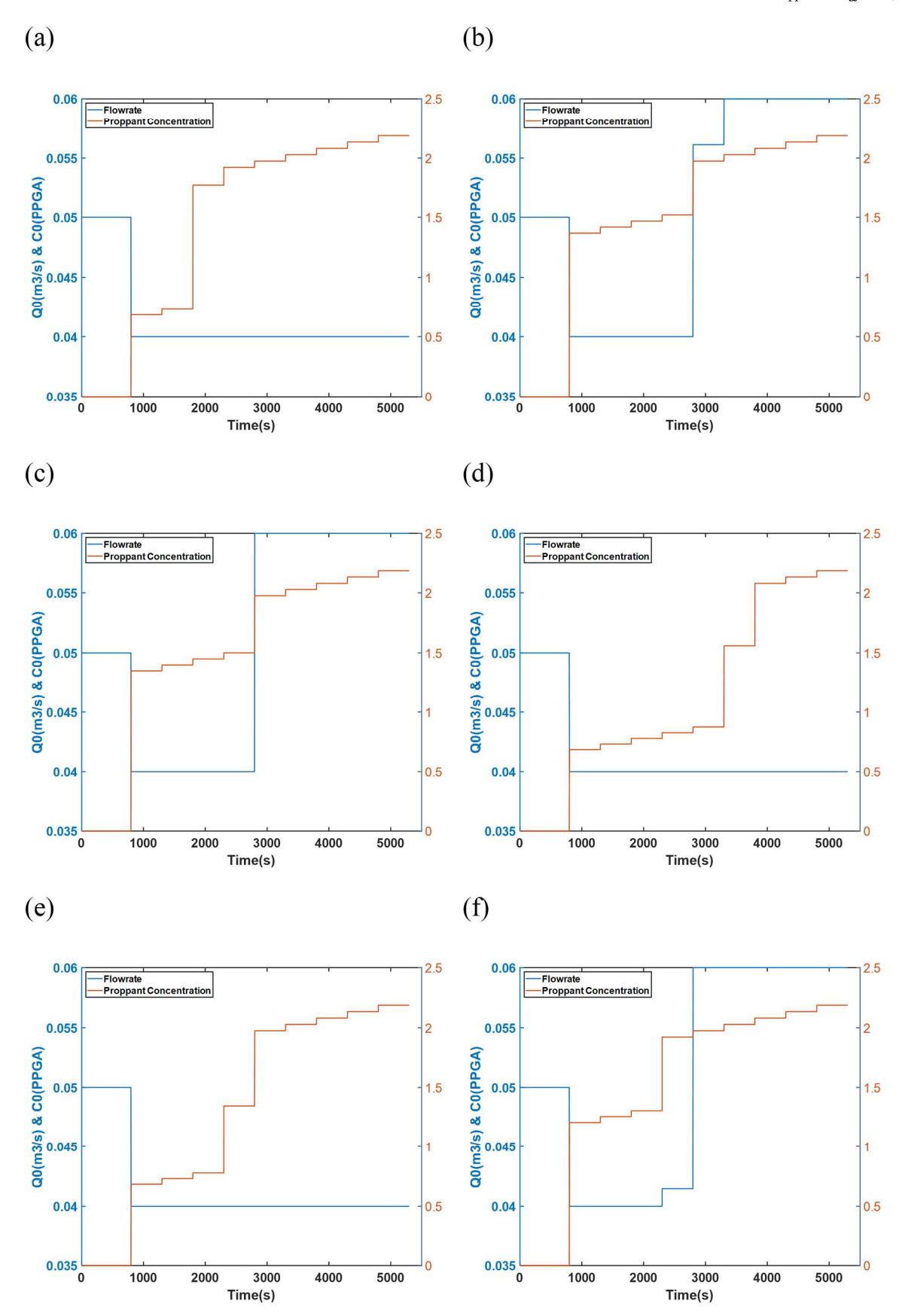


Fig. 11. Optimal pumping profile for each wellpad: (a) wellpad 1, (b) wellpad 2, (c) wellpad 3, (d) wellpad 4, (e) wellpad 5, (f) wellpad 6.

Table 1Detailed designs of hydraulic fracturing operations at the wellpads.

	•					
Description	Pad1	Pad2	Pad3	Pad4	Pad5	Pad6
Freshwater requirement (m^3)	207.07	250.42	252.26	210.00	208.33	252.95
Proppant requirement (kg)	34254	46753	47023	26493	30917	47119
Propped fracture width (10 ⁻⁴ m)	27.32	35.90	36.11	28.48	27.81	36.18
Propped fracture half-length (m)	134.8	140	140	100	119.5	140
Cumulative production (MMm³)	17.65	18.81	18.82	13.15	15.68	18.83

Table 2A detailed description of revenues and costs in the case study.

Description	Value
Gross profit (\$)	6.1818×10^8
Drilling and completion cost (\$)	9.1800×10^6
Shale gas production cost (\$)	1.0387×10^7
Freshwater withdrawal cost (\$)	2.3935×10^6
Freshwater impoundment cost (\$)	6.8475×10^6
Underground reservoir cost (\$)	3.9673×10^4
Proppant acquisition cost (\$)	4.9363×10^6
Natural gas revenue within the scheduling horizon (\$)	$\textbf{8.8173}\times\textbf{10}^{7}$
Natural gas revenue outside the scheduling horizon (\$)	5.6379×10^{8}

5.2. Integrated scheduling and control of hydraulic fracturing operations

To illustrate the performance of the integrated scheduling and control model, a hypothetical case study based on Marcellus Shale Play and the developed superstructure (Fig. 3(a)) is considered. Herein, the case study consists of one interruptible freshwater source, six candidate wellpads, one underground reservoir, and one drilling rig and fracturing crew. The considered scheduling horizon is one year which is discretized into one week time periods. The necessary data for the integrated scheduling and control model are mainly taken from and modified based on the data from Yang et al. [47], Gao and You [4], and Carrero-Parreño et al. [3], which are provided in Table B1 in Appendix B. Note that the major differences among the wellpads lie in the total number of fracturing stages, and completion rate at which the fracturing crew is

capable of performing the fracking, and most importantly, the hydraulic fracturing process. Among them, only the hydraulic fracturing operation recipe is considered variable, which includes the pumping profile and (propped) fracture geometry. In addition, within the scheduling horizon, the freshwater availability, natural gas price, and natural gas demand are time-varying and assumed known, which induces the different hydraulic fracturing operation recipes in different wellpads.

For the integrated problem that is solved offline (i.e., in the design phase), the relaxed MILP problem has 1,116 binary variables, 562,412 continuous variables, and 836,459 constraints. In the reduced MINLP problem, binary variables decrease to 318 since those binary variables representing the schedule of wellpads are fixed based on the solution of the relaxed MILP problem; also, it has 784,636 continuous variables and 544,352 constraints. The relaxed MILP problem is solved using CPLEX 12.9 to a 3% optimality gap in approximately 13,000 s; the reduced MINLP problem is solved using DICOPT 2 with CONOPT 4 and CPLEX 12.9 to a 0% gap in approximately 90 s.

As a result of the case study, the optimal fracturing schedule and the corresponding pumping profiles are presented in Figs. 10 and 11, respectively. The detailed hydraulic fracturing operation designs for the wellpads (i.e., including the freshwater and proppant requirement for a half-fracture, propped fracture width and half-length at the end of pumping, and one-year cumulative shale gas production from a half-fracture) are provided in Table 1. The detailed revenues and costs are provided in Table 2.

Following the obtained fracturing schedule, a gross profit of \$618.18MM was obtained, with \$88.17MM in the revenue of gas production within the one-year scheduling horizon. The underlying logic for this schedule should be three-fold: freshwater availability, natural gas price and natural gas demand. Note that at the end of the one-year horizon, the total revenue (i.e., \$88.17MM) was greater than the associated total costs (i.e., \$33.78MM), which is not common in the industry since it usually takes several years of gas production before the wells can become economically feasible. One possible reason here is that the generally high investment costs for transport system (i.e., pipeline system) and transportation costs (i.e., for freshwater and shale gas) are not considered in this optimization problem.

For the freshwater availability, Fig. 12 illustrates the amount of freshwater pumped and transported to the freshwater impoundments at each wellpad in each week.

As shown in Fig. 12, it can be seen that all the available freshwater except the one in the last two weeks is used for developing the six wellpads. For many of the wellpads, the required freshwater is obtained right before the starting point of their hydraulic fracturing operation to decrease the impoundment operation cost. However, for wellpad 3, the freshwater is pumped and transported to its impoundment starting from

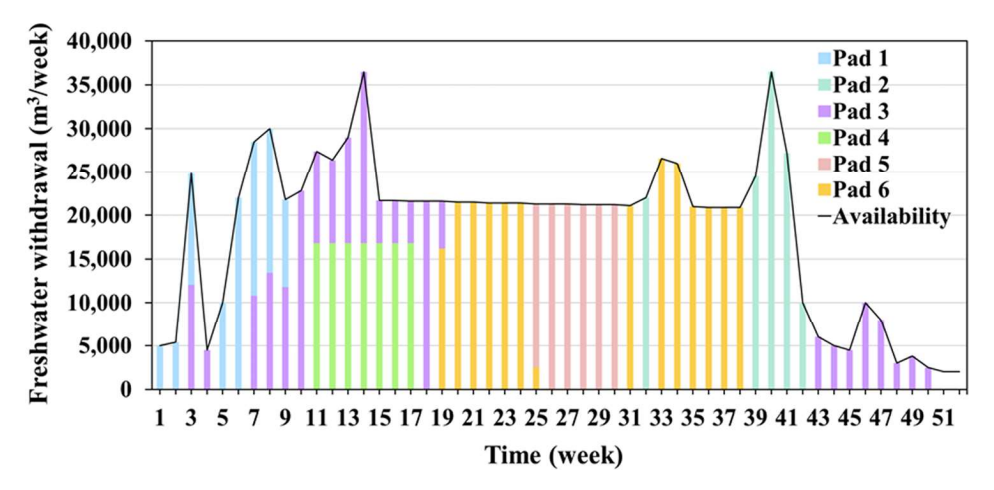


Fig. 12. Freshwater withdrawal for the wellpads over the scheduling horizon.

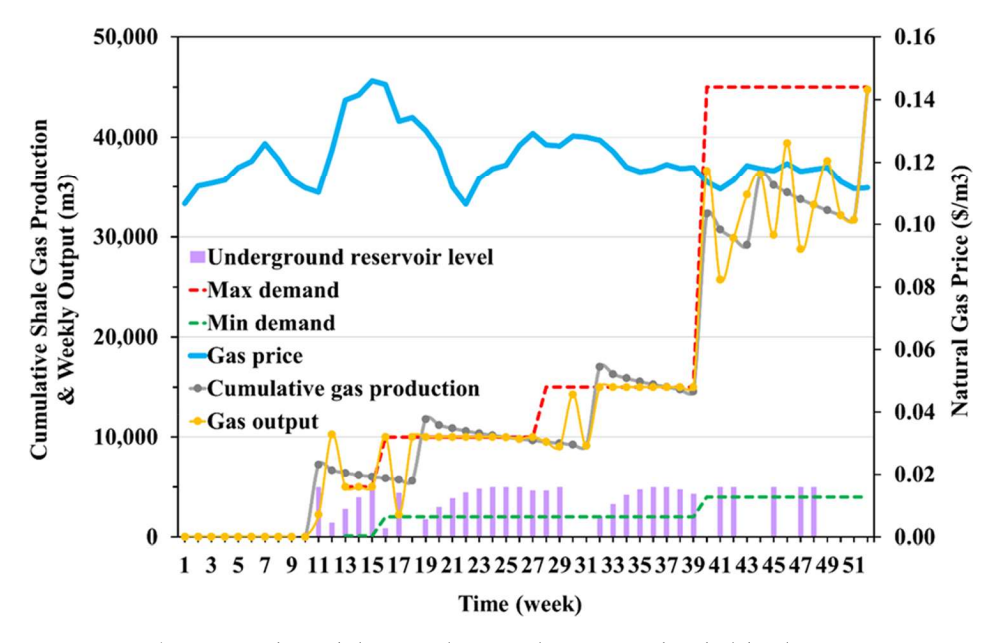


Fig. 13. Cumulative shale gas production and output over the scheduling horizon.

 t_3 (i.e., the purple bar in Fig. 12). This is mainly due to the limited freshwater availability (i.e., only from the interruptible freshwater source). Even though wellpad 3 can be successfully completed with this action, it requires an abnormally large freshwater impoundment in the well site, resulting in the extremely high investment and operating costs. Specifically, its associated impoundment cost accounts for around 32% of the total impoundment cost.

On the other hand, all of the six wellpads are designed to be hydraulic fractured since they are necessary to achieve maximized gross profit while satisfying the natural gas demand. Fig. 13 presents the cumulative shale gas production from the six wellpads and illustrates how the amount of shale gas production sold in each week changes with the varying natural gas demand and price. Here, it is assumed that the timevarying maximum and minimum gas production demands are given to the time period from t_{13} to t_{52} .

At first, to satisfy the production demand in the early stage, wellpad 1 is drilled to allow the shale gas production to start before t_{13} . As shown

in Fig. 13, its production starts in t_{11} ; with the designed pumping profile and fracture geometry, it assures that the maximum demand between t_{13} t_{15} can be achieved. However, since all the shale gas is produced from wellpad 1 before the completion of wellpad 4 in t_{17} , it can be seen that the maximum demand between t_{16} t_{18} cannot always be satisfied due to the decreasing production rate over time. A strategy here is to store most of the shale gas produced in t_{17} temporarily except the part used to satisfy the minimum demand, and then sold them in t_{18} when the natural gas price gets higher. For the same reason, all the stored shale gas production is sold in t_{30} . It should be noted that since the maximum gas demands before t_{40} are relatively low, the hydraulic fracturing operations designed for the wellpads fractured in this period (i.e., t_1 t_{40}) are negatively affected from the economic point of view. Specifically, as shown in Table 1, for wellpads 1, 4, and 5, their designed average propped fracture width and propped fracture half-length are less than the ones designed for wellpads 2, 3, and 6; thus, their resulting shale gas production is lower. The capacity of the underground reservoir also

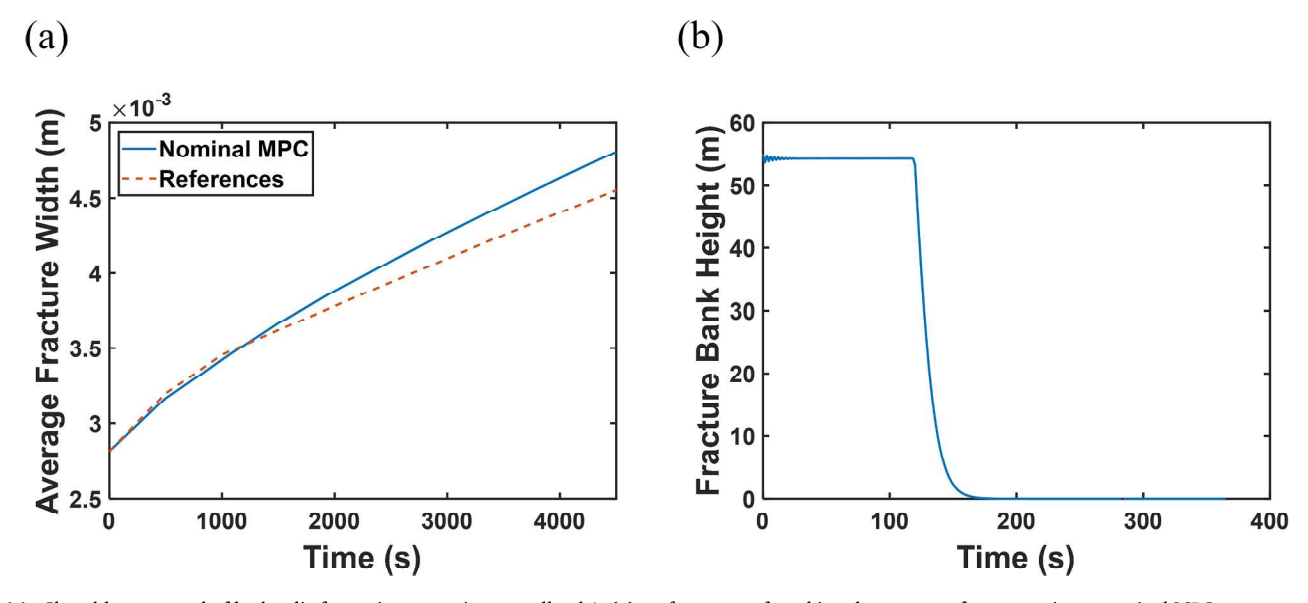


Fig. 14. Closed-loop control of hydraulic fracturing operation at wellpad 1: (a) performance of tracking the output references using a nominal MPC system; and (b) spatial height profile of the resulting proppant bank.

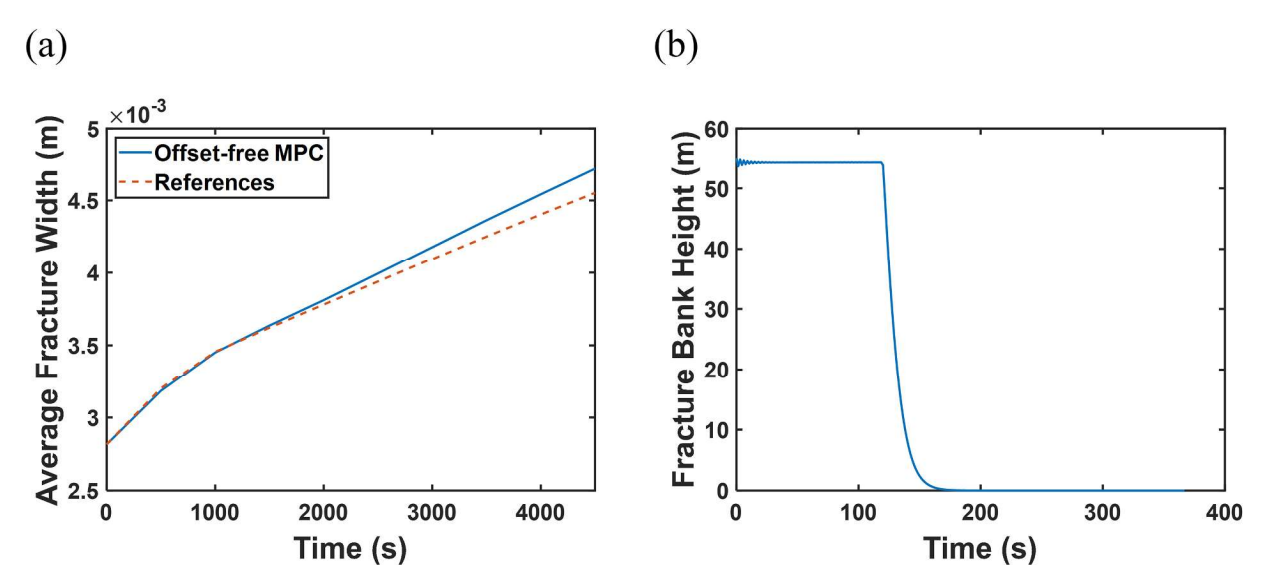


Fig. 15. Closed-loop control of hydraulic fracturing operation at wellpad: 1 (a) performance of tracking the output references using the designed offset-free MPC system; and (b) spatial height profile of the resulting proppant bank.

limits the maximum shale gas production rate at the three wellpads since the maximum capacity is reached in many time periods before t_{40} ; however, the associated operating cost is much less compared to the other costs and thus it may not affect the operation design significantly. As for the three wellpads drilled at last (i.e., wellpad 2, 3, and 6), the objective is mainly to achieve higher revenue of gas production, and thus more water and proppant are required for their hydraulic fracturing operations, as shown in Table 1. Since in this period, the maximum demand is extremely large and thus difficult to be achieved with the limited freshwater availability and underground reservoir capacity, the amount of shale gas sold changes with the natural gas price, as illustrated by the large output in t_{43} , t_{44} , t_{46} , and t_{49} .

Consequently, it is worth mentioning that the formulated integration problem is very general, and thus its application should not be limited to any region (i.e., applicable to a different shale gas play with different resource availability and different product demand and price forecast) and any shale gas network (e.g., considering multiple heterogeneous shale gas wells at each wellpad, multiple rigs and fracturing crews, variable completion rates and number of stages, water management). However, complicating the shale gas network may result in an intractable optimization model, especially when complex connections between the wells/wellpads are taken into consideration (e.g., wastewater reuse/recycling). Further, the online implementation of such a problem becomes computationally inefficient. In this regard, the focuses of our future works would be the application of the proposed framework to large-scale shale gas supply chain networks and the reduction of computation burden.

5.3. Offset-free MPC system

To demonstrate the efficiency of the designed offset-free MPC system for enhanced tracking performance, the closed-loop simulation of hydraulic fracturing operation is performed. First, the dynamic model of the hydraulic fracturing process described in Section 3.1 is utilized as a virtual process. The detailed parameters used for the simulation can be

found in Siddhamshetty et al. [2] In the simulation, the pad time (t_p) is fixed as 800 s as mentioned in Section 5.1. The Kalman filter and control system are initialized at $t=t_p$. In the closed-loop simulation of the hydraulic fracturing operation, the considered sampling time Δ is 500 s. The entire pumping profile is divided into nine pumping stages, and the duration of each stage is exactly equal to the sampling time. Thus, the real-time measurements are available at the beginning of each pumping stage, with which the unmeasurable average fracture width and augmented state of the system can be estimated and then transferred to the control problem to compute the optimal pumping profile online.

Based on the optimal solution from the integrated scheduling and control model which is solved offline as explained in Section 5.2, wellpad 1 should be fracked first, and the desired fracture geometry is known (i.e., output references). Using it as the reference trajectory, a nominal MPC control system without integrating disturbance variables is initially applied, where the controlled variable is only the average fracture width. Herein, two major constraints are considered in the control system: one is that the total amount of the proppant injected should be equal to the designed value from the integrated model; another one is the total amount of the freshwater injected should be equal to or less than the designed value from the integrated model (i.e., the designed amount of proppant and freshwater can be computed using the designed pumping profile determined by the integrated model). Ideally, if the profile of the average fracture width is tracked well with the two constraints satisfied, we are expected to get a fracture with the desired geometry which implies the desired shale gas production profile. Fig. 14 presents the closed-loop results of the nominal MPC for the average fracture width over the hydraulic fracturing operation (i.e., Fig. 14(a)) and the height profile of the proppant bank at the end of pumping (i.e., Fig. 14(b)).

It is observed that the tracking shows poor performance; furthermore, the length of the effective fracture (i.e., the part of the fracture with the proppant bank height around the equilibrium height) is 118.5 m, which is less than the designed value of 134.8 m (as provided in Table 1). One reason for this deviation can be attributed to the

Table 3Comparison of shale gas production between offline design and online design.

	Pad 1	Pad 4	Pad 5
One-year cumulative gas production from a half-fracture (under the offline pumping profile) (MMft³)	15.65	11.49	13.86
One-year cumulative gas production from a half-fracture (under the proposed offset-free MPC system) (MMft³)	15.84	12.47	14.46
One-year cumulative gas production from the entire wellpad (under the designed pumping profile) (MMm³)	212.7	182.2	235.5
One-year cumulative gas production from the entire wellpad (under the offset-free MPC system) (MMm³)	215.4	197.8	245.6
Increase in shale gas production (%)	1.252	8.589	4.281

unavoidable plant-model mismatch from the ROM. Hence, a similar deviation would always exist and reduce the tracking performance. Motivated by this, the designed offset-free MPC is also applied for the regulation of the average fracture width to track the reference trajectory. The obtained results are presented in Fig. 15.

By comparison, with the integrated disturbance variables and chosen B_d and C_d matrices, the tracking performance is improved and thus the effective fracture length can be increased from 118.5 to 120 m. Since the length of the effective fracture is still less than the designed value, the actual shale gas production from wellpad 1 is less than the designed one accordingly. Thus, it should be used as the feedback information for resolving the integrated problem online. This procedure will be explained in Section 5.4 in detail.

Remark 1.. In the offset-free MPC scheme, since the disturbance variables are linearly added to the nominal system, and they are assumed to be constant over the entire control horizon within each iteration of the control loop, the plant-model mismatch in a fed-batch process like hydraulic fracturing, which does not reach steady states, may negatively impact the control/scheduling performance. As a result, it would be challenging to remove the offset of fed-batch processes entirely. Another reason could be the developed linear ROM. Since the controller output references are determined by solving the integrated scheduling and control model in the outer loop where the ROM is used to approximate the original process dynamics for computational efficiency, it is possible that the output reference cannot be perfectly achieved due to the plant-model mismatch.

5.4. Closed-loop implementation with feedback information

To predict the shale gas production rate from a specific wellpad, the CMG-GEM software is used. Herein, the required inputs are the propped fracture length, propped fracture width, and the propped fracture height. According to the optimal solution of the offline integrated problem (Section 5.2), wellpad 1 is hydraulic fractured first. By directly implementing the optimal pumping profile shown in Fig. 11(a) to the process (i.e., high-fidelity model is used as a virtual process), the spatiotemporal evolution of fracture width and proppant bank height can be obtained, with which the actual average propped fracture width and propped fracture length are computed as 0.004999 m and 118.5 m, respectively. As a result, the forecasted one-year cumulative shale gas production from a half-fracture at wellpad 1 is estimated to be 15.65 MMft³. However, even with the same amount of freshwater and proppant consumption, the cumulative production can be enhanced up to 15.84MMft³ by utilizing the designed offset-free MPC system (Fig. 15 (a)). Additionally, as shown in Table 3, the one-year cumulative shale gas production from both a half-fracture and the entire wellpad has increased when implementing the designed offset-free MPC system (online) compared to the offline implementation of pumping profiles.

In other words, the proposed online integrated framework in this study enhanced the shale gas production. This is because the online implementation considers feedback information, which allows the scheduling and controller output references to be updated timely during the shale gas production to cope with the deviation between the designed and the actual case. Hence, a potential loss in the total gas production revenue can be avoided.

6. Conclusions

In this study, a closed-loop framework for the integration of scheduling and control, which has been implemented in the hydraulic fracturing process, is developed. The goal is to obtain a better assessment of shale gas resources by considering the pumping profile design when determining the optimal fracturing schedule for shale gas development. For this, a ROM is constructed based on the simulation data from a highfidelity hydraulic fracturing model, which is further integrated with the scheduling model. Herein, the linking variables are the amounts of freshwater and proppant requirement, and shale gas production. By utilizing the ROM, the computation complexity of the integrated scheduling and control problem is significantly alleviated, hence, the scheduling and control decisions are determined simultaneously and efficiently. However, the existing plant-model mismatch results in a large economic loss when implementing the offline decisions online. Thus, the integrated scheduling and control model is solved to determine the controller output references instead of process inputs; subsequently, the offset-free MPC is employed online to track the reference trajectory from the integrated model. Furthermore, by incorporating the disturbances into the control system, the influences of plant-model mismatch can be alleviated while the online control solutions still satisfy the operational constraints. Consequently, the designed offsetfree MPC system allows the reference trajectory to be better tracked in comparison to the nominal MPC system; with the proposed online integrated framework, the economic loss in the shale gas system caused by the plant-model mismatch can be largely prevented. Furthermore, future prospects are able to provide the application of the proposed approach to a large-scale and complex shale gas system, and the extension of the framework to include planning decisions.

Declaration of Competing Interest

The authors declare that they have no known competing financial interests or personal relationships that could have appeared to influence the work reported in this paper.

Appendix A. Input parameters for shale gas production simulation

See Table A1

Table A1Necessary shale gas reservoir parameters used for the shale gas production simulation [46].

Parameter	Value
Model dimension ($x \times y \times z$, ft)	200 × 2,000 × 196.8504
Initial reservoir pressure (psi)	4,300
Bottomhole pressure (psi)	1,000
Reservoir temperature (°F)	130
Reservoir permeability (md)	0.00005
Reservoir porosity (%)	10
Residual water saturation (%)	10
Total compressibility (psi ⁻¹)	$3 imes10^{-6}$

Appendix B. Input parameters for the case study

See Table B1

Table B1Necessary parameters and cost coefficients used for the case study [3,4,47].

Parameter	Value
Total number of fracturing stages (-)	$i_1:120;\ i_2:120;\ i_3:210;\ i_4:140;\ i_5:150;\ i_6:280$
Completion rate (stages/ week)	$i_1: 20; \ i_2: 40; \ i_3: 30; \ i_4: 20; \ i_5: 30; \ i_6: 40$
Number of fractures per stage (-)	2
Drilling and completion cost (\$)	$1,080,000 \sim \ 2,520,000$
Shale gas production cost (\$/m³)	0.014
Freshwater withdrawal cost (\$/m³)	2.5
Proppant acquisition cost (\$/ton)	30
Freshwater availability (m³/week)	$2,000 \sim 36,500$
Base investment cost for impoundment (\$)	360,000
Incremental investment cost for impoundment (\$/m³)	7.4
Operating cost for impoundment (\$/week)	10,500
Working gas capacity of underground reservoir (m³/week)	5,000,000
Unit injection cost at underground reservoir (\$/mcf)	0.02
Unit withdrawal cost at underground reservoir (\$/mcf)	0.01
Natural gas price within the scheduling horizon (\$/m³)	0.106 ~ 0.146
Natural gas price outside the scheduling horizon $(\$/m^3)$	0.1
Natural gas demand (m³/week)	$100,000 \sim \ 45,000,000$

References

- EIA. Annual Energy Outlook 2018 with projections to 2050. Washington, DC: U.S. Energy Information Administration (EIA); 2018.
- [2] Siddhamshetty P, Kwon JS, Liu S, Valkó PP. Feedback control of proppant bank heights during hydraulic fracturing for enhanced productivity in shale formations. AIChE J 2018;64:1638–50.
- [3] Carrero-Parreño A, Reyes-Labarta JA, Salcedo-Díaz R, Ruiz-Femenia R, Onishi VC, Caballero JA, et al. Holistic planning model for sustainable water management in the shale gas industry. Ind Eng Chem Res 2018;57:13131–43.
- [4] Gao J, You F. Shale gas supply chain design and operations toward better economic and life cycle environmental performance: MINLP model and global optimization algorithm. ACS Sustain Chem Eng 2015;3:1282–91.
- [5] Cafaro DC, Grossmann IE. Strategic planning, design, and development of the shale gas supply chain network. AIChE J 2014;60(6):2122–42.
- [6] Drouven MG, Grossmann IE. Multi-period planning, design, and strategic models for long-term, quality-sensitive shale gas development. AIChE J 2016;62: 2296–323.
- [7] Chebeir J, Asala H, Manee V, Gupta I, Romagnoli JA. Data driven techno-economic framework for the development of shale gas resources. J Nat Gas Sci Eng 2019;72: 103007.
- [8] Guerra OJ, Calderón AJ, Papageorgiou LG, Siirola JJ, Reklaitis GV. An optimization framework for the integration of water management and shale gas supply chain design. Comput Chem Eng 2016;92:230–55.

- [9] Ahn Y, Siddhamshetty P, Cao K, Han J, Kwon JS. Optimal design of shale gas supply chain network considering MPC-based pumping schedule of hydraulic fracturing in unconventional reservoirs. Chem Eng Res Des 2019;147:412–29.
- [10] Ahn Y, Kim J, Kwon JS. Optimal design of supply chain network with carbon dioxide injection for enhanced shale gas recovery. Appl Energy 2020;274:115334.
- [11] Cao K, Siddhamshetty P, Ahn Y, El-Hawagi M, Kwon JS. Evaluating the spatiotemporal variability of water recovery ratios of shale gas wells and their effects on shale gas development. J Clean Prod 2020;276:123171.
- [12] Chen Y, He L, Li J, Zhang S. Multi-criteria design of shale-gas-water supply chains and production systems towards optimal life cycle economics and greenhouse gas emissions under uncertainty. Comput Chem Eng 2018;109:216–35.
- [13] Yang L, Grossmann IE, Manno J. Optimization models for shale gas water management. AIChE J 2014;60:3490–501.
- [14] Drouven MG, Grossmann IE. Mixed-integer programming models for line pressure optimization in shale gas gathering systems. J Pet Sci Eng 2017;157:1021–32.
- [15] Knudsen BR, Grossmann IE, Foss B, Conn AR. Lagrangian relaxation based decomposition for well scheduling in shale-gas systems. Comput Chem Eng 2014; 63:234–49.
- [16] Knudsen BR, Whitson CH, Foss B. Shale-gas scheduling for natural-gas supply in electric power production. Energy 2014;78:165–82.
- [17] Cafaro DC, Drouven MG, Grossmann IE. Optimization models for planning shale gas well refracture treatments. AIChE J 2016;62:4297–307.
- [18] Cafaro DC, Drouven MG, Grossmann IE. Continuous-time formulations for the optimal planning of multiple refracture treatments in a shale gas well. AIChE J 2018;64:1511–6.
- [19] Ondeck A, Drouven M, Blandino N, Grossmann IE. Multi-operational planning of shale gas pad development. Comput Chem Eng 2019;126:83–101.
- [20] Wilson KC, Durlofsky LJ. Optimization of shale gas field development using direct search techniques and reduced-physics models. J Pet Sci Eng 2013;108:304–15.
- [21] Forouzanfar F, Reynolds AC. Joint optimization of number of wells, well locations and controls using a gradient-based algorithm. Chem Eng Res Des 2014;92: 1315–28.
- [22] Liu S, Valkó PP. Optimization of spacing and penetration ratio for infinite-conductivity fractures in unconventional reservoirs: a section-based approach. SPE J 2017;22:1–877.
- [23] Ma X, Plaksina T, Gildin E. Optimization of placement of hydraulic fracture stages in horizontal wells drilled in shale gas reservoirs. In: Unconventional Resources Technology Conference. Society of Exploration Geophysicists, American Association of Petroleum Geologists, Society of Petroleum Engineers; 2013, p. 1479–89.
- [24] Yu W, Sepehrnoori K. Optimization of multiple hydraulically fractured horizontal wells in unconventional gas reservoirs. J Pet Eng 2013;2013.
- [25] Siddhamshetty P, Yang S, Kwon JS. Modeling of hydraulic fracturing and designing of online pumping schedules to achieve uniform proppant concentration in conventional oil reservoirs. Comput Chem Eng 2018;114:306–17.
- [26] Siddhamshetty P, Wu K, Kwon JS. Modeling and Control of Proppant Distribution of Multistage Hydraulic Fracturing in Horizontal Shale Wells. Ind Eng Chem Res 2019;58:3159-69.
- [27] Cao K, Siddhamshetty P, Ahn Y, Mukherjee R, Kwon JS. Economic model-based controller design framework for hydraulic fracturing to optimize shale gas production and water usage. Ind Eng Chem Res 2019;58(27):12097–115.
- [28] Flores-Tlacuahuac A, Grossmann IE. Simultaneous cyclic scheduling and control of a multiproduct CSTR. Ind Eng Chem Res 2006;45:6698–712.
- [29] Terrazas-Moreno S, Flores-Tlacuahuac A, Grossmann IE. Simultaneous cyclic scheduling and optimal control of polymerization reactors. AIChE J 2007;53: 2301–15.
- [30] Nyström RH, Franke R, Harjunkoski I, Kroll A. Production campaign planning including grade transition sequencing and dynamic optimization. Comput Chem Eng 2005;29:2163–79.
- [31] Nyström RH, Harjunkoski I, Kroll A. Production optimization for continuously operated processes with optimal operation and scheduling of multiple units. Comput Chem Eng 2006;30:392–406.
- [32] Baldea M, Harjunkoski I. Integrated production scheduling and process control: A systematic review. Comput Chem Eng 2014;71:377–90.
- [33] Terrazas-Moreno S, Flores-Tlacuahuac A, Grossmann IE. Lagrangean heuristic for the scheduling and control of polymerization reactors. AIChE J 2008;54:163–82.
- [34] Chu Y, You F. Integrated scheduling and dynamic optimization of complex batch processes with general network structure using a generalized benders decomposition approach. Ind Eng Chem Res 2013;52:7867–85.
- [35] Nie Y, Biegler LT, Villa CM, Wassick JM. Discrete time formulation for the integration of scheduling and dynamic optimization. Ind Eng Chem Res 2015;54: 4303–15.
- [36] Chu Y, You F. Integrated scheduling and dynamic optimization by stackelberg game: bilevel model formulation and efficient solution algorithm. Ind Eng Chem Res 2014;53:5564–81.
- [37] Valdez-Navarro YI, Ricardez-Sandoval LA. A novel back-off algorithm for integration of scheduling and control of batch processes under uncertainty. Ind Eng Chem Res 2019;58:22064–83.
- [38] Zhuge J, Ierapetritou MG. Integration of scheduling and control for batch processes using multi-parametric model predictive control. AIChE J 2014;60:3169–83.
- [39] Burnak B, Pistikopoulos EN. Integrated process design, scheduling, and model predictive control of batch processes with closed-loop implementation. AIChE J 2020;66:e16981.
- [40] Zhuge J, Ierapetritou MG. An integrated framework for scheduling and control using fast model predictive control. AIChE J 2015;61:3304–19.

- [41] Dias LS, Ierapetritou MG. From process control to supply chain management: An overview of integrated decision making strategies. Comput Chem Eng 2017;106: 826–35
- [42] Zhuge J, Ierapetritou MG. Integration of scheduling and control with closed loop implementation. Ind Eng Chem Res 2012;51:8550–65.
- [43] Chu Y, You F. Moving horizon approach of integrating scheduling and control for sequential batch processes. AIChE J 2014;60:1654–71.
- [44] Pannocchia G, Rawlings JB. Disturbance models for offset-free model-predictive control. AIChE J 2003;49:426–37.
- [45] Pannocchia G. Offset-free tracking MPC: A tutorial review and comparison of different formulations. In: 2015 European control conference (ECC). IEEE; 2015, p. 527–32.
- [46] Mao S, Siddhamshetty P, Zhang Z, Yu W, Chun T, Kwon JS, et al. Impact of Proppant Pumping Schedule on Well Production for Slickwater Fracturing. SPE J 2021;26:342–58.
- [47] Yang L, Grossmann IE, Mauter MS, Dilmore RM. Investment optimization model for freshwater acquisition and wastewater handling in shale gas production. AIChE J 2015;61:1770–82.